Formal Hydrogen Transfer Reactions and the Effects of Non-Redox Active Metal Cations

by

Jeffrey A. van Santen

B.Sc. Hons. Chemistry, The University of British Columbia, 2015

A THESIS SUBMITTED IN PARTIAL FULFILLMENT OF
THE REQUIREMENTS FOR THE DEGREE OF

MASTER OF SCIENCE

in

THE COLLEGE OF GRADUATE STUDIES

(Chemistry)

THE UNIVERSITY OF BRITISH COLUMBIA

(Okanagan)

June 2017

The undersigned certify that they have read, and recommend to the College of Graduate Studies for acceptance, a thesis entitled: Formal Hydrogen Transfer Reactions and the Effects of Non-Redox Active Metal Cations submitted by Jeffrey A. van Santen in partial fulfilment of the

requirements of the degree of Master of Science

Supervisor, Professor (please print name and faculty/school above the line)

Supervisory Committee Member, Professor (please print name and faculty/school above the line)

Supervisory Committee Member, Professor (please print name and faculty/school above the line)

University Examiner, Professor (please print name and faculty/school above the line)

External Examiner, Professor (please print name and faculty/school above the line)

(Date Submitted to Grad Studies)

Additional Committee Members include:

(please print name and faculty/school above the line)

(please print name and faculty/school above the line)

Abstract

This is a sample thesis based on the `ubcthesis.cls` template from Michael Forbes. The thesis includes the additional style file `ubcostyle.sty` in accordance to the official standards for the UBCO College of Graduate Studies. This sample thesis together with the style files and templates produces a document that is officially accepted by the UBCO College of Graduate Studies.

If you need a package, look into ubcostyle.sty to see if it is not already loaded there. See the file README.txt for additional instructions to produce the bibliography, index, and glossary automatically.

Preface

Preface stuff

If any part of your thesis was co-written, you must include a Co-Authorship statement. Also indicate if part of the thesis was published with the reference.

Table of Contents

Abstract . . . . . **iii**

Preface . . . . . **iv**

List of Tables . . . . . **viii**

List of Figures . . . . . **ix**

List of Schemes . . . . . **x**

List of Symbols and Abbreviations . . . . . **xi**

Acknowledgements . . . . . **xiii**

Dedication . . . . . **xiv**

Chapter 1: Introduction **1**
1.1 Processes involving hydrogen transfer reactions 1
1.1.1 Hydrogen atom transfer reactions in biological processes 1
1.1.2 Hydrogen atom transfer reaction in chemical processes 4
1.2 Physico-chemical determinants of formal hydrogen transfer reactions 6
1.2.1 Understanding chemical reactions 6
1.2.2 Factors influencing the kinetics of HAT reactions . . . 7
1.2.3 Mechanistic details of hydrogen transfer reactions . . . 12
1.2.4 The effects of metal cations on HAT reactions 15

Chapter 2: Theory **18**
2.1 The quantum mechanical approach 18
2.1.1 Spin and Spatial Orbitals 19
2.1.2 The Hartree product 19

2.1.3 Slater determinants 20
2.1.4 The Hartree-Fock approximation 21
2.1.5 Basis sets 22
2.1.6 Post-Hartree-Fock methods 26
2.1.7 The complete basis set limit 29
2.1.8 Composite quantum chemistry methods 30
2.1.9 Density-functional theory 30
2.2 Applying theory to chemical problems 33
2.2.1 Geometry optimisation 33
2.2.2 Molecular vibrations 34
2.2.3 Thermochemistry 35
2.2.4 Modelling solvent 37
2.2.5 Rate constants and transition state theory 38

Chapter 3: Methods 45
3.1 Chapter 4 45
3.2 Chapter 5 46
3.3 Chapter 6 48
3.3.1 Benchmark study of non-redox active metal cations with organic substrates 48
3.3.2 Effects of metal cations on hydrogen atom transfer barrier heights 49

Chapter 4: The Relationship Between Arrhenius Pre-factors with Non-Covalent Binding 50

Chapter 5: Interrogation of the Bell-Evans-Polanyi Principle: Investigation of the Bond Dissociation Enthalpies correlated with Hydrogen Atom Transfer Rate Constants 51

Chapter 6: Do non-redox active metal cations have the potentials to behave as chemo-protective agents? The Effects on Metal Cations on HAT Reaction Barrier Heights 52
6.1 Benchmarking Density Functional Theory for the Binding of Alkali and Alkaline Earth Metals 52
6.1.1 Methods 53
6.1.2 Benchmark systems 54
6.1.3 Metal cation basis set convergence 55

6.1.4 High level results and evaluation of various density-functional theory methods 55

Chapter 7: Conclusion 57

References 59

Appendix 73

List of Tables

Table 1.1 Summary of second-order rate constants for HAT from C-H bonds for hydrogen bond accepting substrates from the cumyloxyl radical. 8
Table 1.2 Summary of experimental rate constants of HAT with CumO$^{\bullet}$ for cyclohexadiene (CHD), tetrahyrofuran (THF), triethylamine (TEA), and 1,2,2,6,6-pentamethylpiperidine (PMP), including the effect of non-redox active metal cations. 16

List of Figures

Figure 1.1 Placeholder PES from Wikipedia 6
Figure 1.2 Energy profiles for a series of related exothermic reactions illustrating the Bell-Evans-Polanyi Principle. . 11
Figure 1.3 Plots of observed rate constants against concentration of substrate for HAT reactions with cumyloxyl radical. 17

Figure 2.1 A reaction coordinate diagram for a generic reaction. 40
Figure 2.2 Quantum mechanical tunnelling occurs when a particle penetrates a reaction barrier, rather than surmounting it. (Place holder figure) 43

Figure 3.1 Example locally dense basis set partitioning on benzene used in the LDBS approach. 47

List of Schemes

1.1 Common reactions involved in radical-mediated oxidation of proteins . . . 3
1.2 Reaction mechanism of the Hofmann-Löfler-Freytag reaction . 5
1.3 A generic HAT transition state structures and possible resonance forms. . . . 12
1.4 A generic formal hydrogen transfer reaction. . . . 13
1.5 Self-exchange reactions of the **A.** benzyl/toluene couple through direct HAT **B.** phenoxyl/phenol couple through PCET. . . . 13

6.1 Binding of the calcium cation (Ca^{2+}) to the oxygen lone pairs of N,N-dimethylacetamide. . . . 53
6.2 Initial proposed benchmark set of molecules and cations. Note this set consistes of all combinations of substrates and metal cation, thus there are 60 complexes in the set. . . . 55
6.3 Revised benchmark set of small substrates and cations. Note this set consistes of all combinations of substrates and metal cation, thus there are 35 complexes in the set. . . . 56

List of Symbols and Abbreviations

BDE	bond dissociation enthalpy
BEP	Bell-Evans-Polanyi
$BnO^{\bullet}$	benzyloxyl radical
CHD	cyclohexadiene
$CumO^{\bullet}$	cumyloxyl radical
DFT	density-functional theory
DNA	deoxyribonucleic acid
DMA	N,N-dimethylacetamide
DMF	N,N-dimethylformamide
E_a	activation energy
FHT	formal hydrogen transfer
$\mathscr{H}$	Hamiltonian operator
HAT	hydrogen atom transfer
HB	hydrogen bond
HF	Hartree-Fock
HOMO	highest occupied molecular orbital
kcal mol^{-1}	kilocalories per mole
K_x	equilibrium constant
k_x	rate constant
KSEs	kinetic solvent effects
LFER	linear free energy relationship
LFP	laser flash photolysis
M	molar concentration
MO	molecular orbital
MDA	malondaldehyde
NCI	non-covalent interaction
PCET	proton coupled electron transfer
PMP	1,2,2,6,6-pentamethylpiperadine
PES	potential energy surface
RNA	ribonucleic acid
ROS	reactive oxygen species
s	seconds
SOMO	singly occupied molecular orbital
SPLET	sequential proton loss electron transfer
STO	Slater-type orbital
TEA	triethylamine
THF	tetrahydrofuran
TS	transition state
Z	atomic number

Acknowledgements

This is the place to thank professional colleagues and people who have given you the most help during the course of your graduate work.

Dedication

The dedication is usually quite short, and is a personal rather than an academic recognition. The *Dedication* does not have to be titled, but it must appear in the table of contents. If you want to skip the chapter title but still enter it into the Table of Contents, use this command `\chapter[Dedication]{}`.

Chapter 1

Introduction

Hydrogen atom transfer (HAT) reactions involve chemical species with an odd number of electrons, or free radicals. These fundamental chemical transformations have been studied extensively for over a century.[1,2] All HAT reactions involve the transfer of at least one hydrogen atom ($H^{\bullet}$), although there exist various mechanisms by which this can occur. Free radicals and HAT reactions play an important role in many chemical and biological processes.[3]

1.1 Processes involving hydrogen transfer reactions

1.1.1 Hydrogen atom transfer reactions in biological processes

In biology, oxygen centred radicals are referred to as reactive oxygen species (ROSs). Nearly all ROSs derive from the metabolic processes involving molecular oxygen, O_2.[4] At conditions relevant to biology, organic matter exists in the singlet ground state while O_2 exists in a triplet ground state: the quantum mechanical selection rule prohibits electronic interactions. As a result, evolution has driven organisms to develop techniques to overcome this. Most commonly, enzymes containing transition metals are used to activate O_2, producing reactive radical intermediates or products, i.e. ROSs. ROSs play an important role in normal biological functions, however an "imbalance" may lead to the oxidation of important biomaterials, or oxidative stress.[3] In humans, oxidative stress has been linked to many degenerative disease states such as Alzheimer's disease,[4,5] Parkinson's disease,[6] ageing, and cancer.[7]

It is widely accepted that the vast majority of ROSs originate from reactions of O_2 with the redox-active metals copper and iron.[3] A common example is the Haber-Weiss reaction, the second step in the Fenton cycle (Equations 1.1 - 1.3):

$$Fe^{3+} + {}^{\bullet}O_2^- \longrightarrow Fe^{2+} + O_2 \quad (1.1)$$

$$Fe^{2+} + H_2O_2 \longrightarrow Fe^{3+} + OH^- + {}^{\bullet}OH \quad (1.2)$$

$$\overline{\qquad\qquad\qquad\qquad\qquad\qquad\qquad\qquad}$$

$${}^{\bullet}O_2^- + H_2O_2 \longrightarrow {}^{\bullet}OH + OH^- + O_2 \quad (1.3)$$

It is the production of the highly reactive hydroxyl radical ($^{\bullet}$OH) which is responsible for the initiation of the majority of oxidative stress through the abstraction of a hydrogen atom. Given its very short *in vivo* half-life of about 10^{-9} s, $^{\bullet}$OH reacts with practically all biomaterials.[8]

DNA and RNA are susceptible to radical damage,[3,5] and reactions of $^{\bullet}$OH with DNA molecules have been studied in some detail. Damage can occur to both the pyrimidine and purine bases, as well as the deoxyribose backbone, with over 20 DNA lesions having been identified.[9,10] The most commonly studied product is 8-hydroxyguanine (or the tautomer 8-oxo-2′-deoxyguanosine), which is the result of the oxidation of the guanine nitrogenous base. This particular oxidation can result in mismatched base pairing of guanosine with adenine (rather than cytosine), contrary to the Watson-Crick model, leading to possible substitutions in the genome.[11] It is important to realise that although there are enzymes which actively repair DNA and remove lesions,[12] oxidation represents the permanent modification of genetic material which is the first step in mutagenesis, carcinogenesis, and ageing.

Polyunsaturated fatty acids are extremely sensitive to oxidation. Specifically, the autoxidation of polyunsaturated fatty acids and esters occurs rapidly, and has been intensely investigated.[13–17] This radical chain reaction is initiated by reactions of lipids with $^{\bullet}$OH forming a pentadienyl radical. Oxygen adds rapidly (although reversibly) to the intermediate carbon radical,[15] giving a lipid peroxyl radical (LOO$^{\bullet}$). Once formed, LOO$^{\bullet}$ can propagate to form further carbon centred radicals, terminate through the reaction with another LOO$^{\bullet}$, or can rearrange through a cyclisation reaction to form an endoperoxide. The endoperoxide product reacts further to produce mainly aldehydes, and most predominantly malondialdehyde (MDA).[5] MDA is highly reactive and has been shown to be either mutagenic or carcinogenic in mammalian and bacterial models.[13]

Our work is primarily concerned with models for proteins. The oxidation of protein by ROSs occurs through a radical chain mechanism which has been studied in detail.[18] Through experiments in which proteins were exposed to ionising radiation, it was demonstrated that protein oxidation is

initiated through hydrogen atom transfer (HAT) reactions with $^{\bullet}$OH. The propagation often occurs through radical-mediated oxidation, as illustrated in Scheme 1.1.

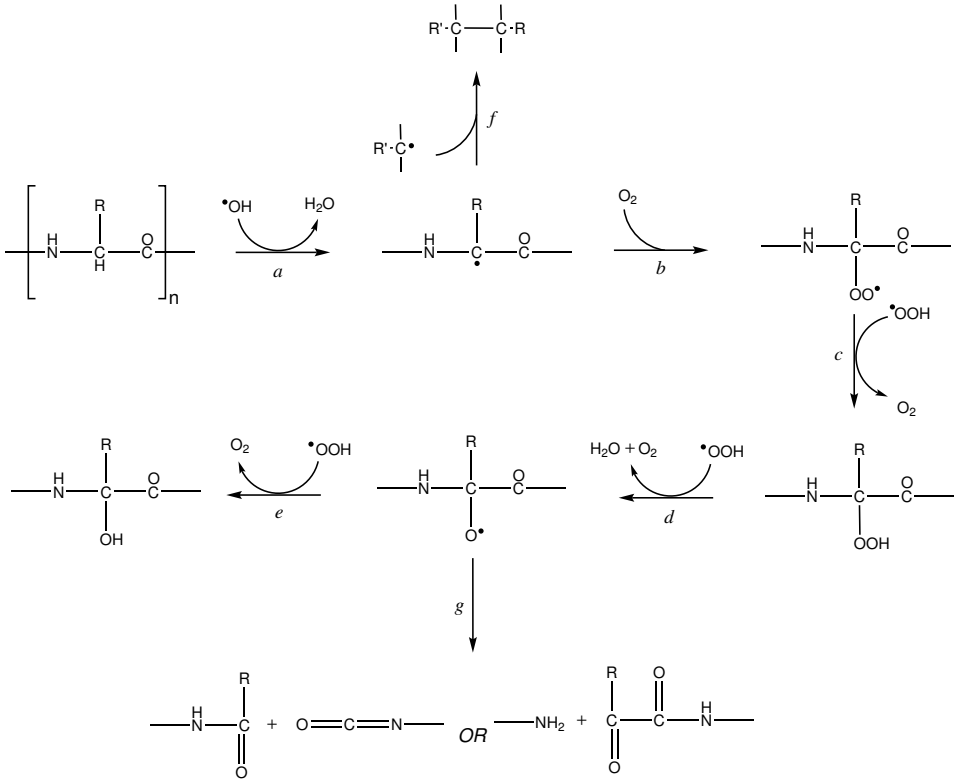

Scheme 1.1: Common reaction involved in radical-meditated oxidation of proteins. The reactions are as follows: *a* initiation or radical chain through abstraction by the hydroxyl radical, *b* radical addition of molecular oxygen, *c* HAT with an incipient peroxyl radical, *d* additional reaction with an incipient peroxyl radical producing water and oxygen, *e* termination by HAT with an incipient peroxyl radical, *f* possible cross-linking mechanism of two carbon centred radicals *g* possible fragmentation pathways of an oxygen centred radical intermediate. Figure adapted from Reference 18.

Initial abstraction occurs primarily at the α-carbon position (Reaction *a*), although the side-chains are also susceptible to oxidation. Those side-chains containing sulfur,[19] as well as tyrosine (which has a fairly weak phenolic O-H bond of about 89 kcal mol^{-1}),[20] are particularly susceptible to

oxidation. The course of propagation through radical mediated protein oxidation is determined by the availability of either singlet oxygen ($^1O_2$), or superoxide ($O_2^{\bullet -}$) (or the protonated form, hydroxyl radical ($^{\bullet}OOH$)). Reactions that proceed with singlet oxygen are shown in *b* - *e*. The radical chain reaction can be terminated through two mechanisms, protein-protein cross-linking (Reaction *f*) or protein fragmentation (Reaction *g*). These processes lead to the accumulation of oxidised proteins which is associated with many degenerative diseases.[21]

1.1.2 Hydrogen atom transfer reaction in chemical processes

Given the importance of HAT reaction in biological systems, it seems obvious for chemists to develop means in which this tool can be used as well. Given the highly reactive nature of free radicals, this has certainly been a challenge. However, there exists multiple examples of utilising HAT reactions in important energy conversion processes,[22] as well as in chemical synthesis.[23,24]

In organic synthesis, the replacement of specific C-H bonds (C-H bond functionalisation) has long been of interest. One such way to achieve this is through radical reactions.[25] Intramolecular radical reactions were first utilised in the late 1800s when Hofmann showed that homolysis of bromamines and chloramines lead to functionalisation of δ-methylene or methyl groups.(citation needed, see Godula and Sames[25]) Now called the Hofmann-Löfler-Freytag reaction, this reaction is used to form cyclic amines, and proceeds through an intramolecular HAT, as shown in Scheme 1.2. The reaction is initiated by the cleavage of a nitrogen-halogen bond, either by radiation or a radical initiator. Next is a key intramolecular HAT reaction that proceeds through a six-membered cyclic transition state which can adopt an unstrained chair conformation. Another related reaction is the Barton reaction[26] which involves photo-initiated homolytic cleavage of a nitrite (RO-NO) bond, followed by δ-hydrogen abstraction, and radical coupling to form a δ-nitroso alcohol. The Hofmann-Löfler-Freytag reaction served as a proof of concept that HAT could be useful in synthetic chemistry.

Since the early days of Hofmann, a great deal of work has been done, and new methods for C-H functionalisation have been achieved. The most commonly used technique is the hydroxylation of C-H bonds, which then serve as a synthetic handle. Transition metal chemistry is now typically employed to achieve C-H bond functionalisation. This often involves highly reactive metal-oxo intermediates responsible for triggering C-H bond cleavage,

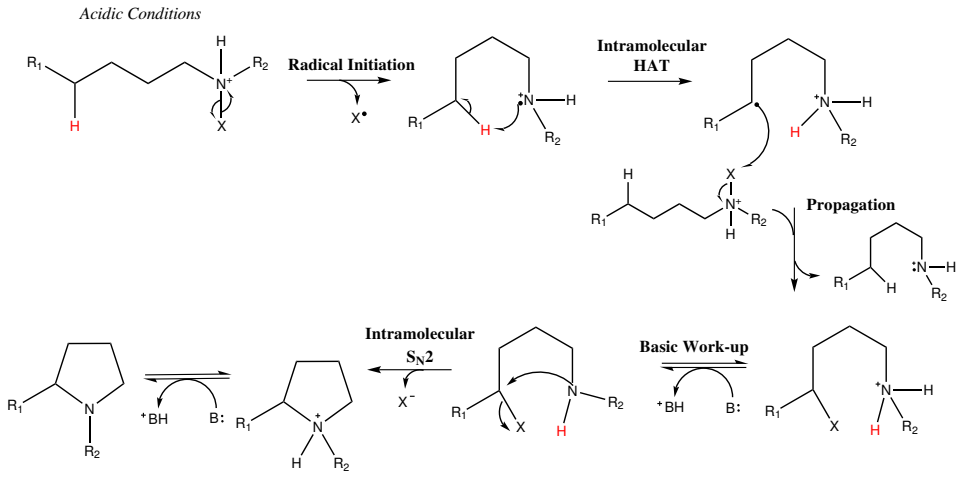

Scheme 1.2: Reaction mechanism of the Hofmann-Löfler-Freytag reaction. The reaction proceeds under acidic conditions so that the amine is protonated. Step one is radical initiation, typically through radiation or a radical initiator, step two is the intramolecular HAT reaction, step three is the propagation of the radical activating addition amines and abstracting a halide, step four begins the basic work up with deprotonation of the amine, followed by S_N2 attack of the δ position with a halide, and finally the second deprotonation of the amine centre.

with an inorganic HAT reaction being an essential part of the mechanism.[27] Reactions of this nature are subject to low selectivity and complex product mixtures due to the similarly thermodynamics and kinetics of hydroxylation and dehydrogenation pathways.[23] A similar mechanism is found in metalloenzymes, which prompted important work investigating the selectivity and tunability of these reactions, with considerable success. This work along several works of others,[24] are exemplary cases where a detailed understanding of the HAT reaction mechanism can lead to significant contributions to chemistry.

1.2 Physico-chemical determinants of formal hydrogen transfer reactions

Given the importance of HAT reactions in biology and chemistry, a thorough understanding of these reactions is clearly important. In order to fully understand HAT reactions, we much understand the factors which influence these reactions.

1.2.1 Understanding chemical reactions

The potential energy surface (PES) for any chemical reaction is a complex hypersurface that depends on many variables. Typically this problem can be simplified by examining only the relevant geometry changes. Often the two most important coordinates can be isolated, giving a 3-dimensional potential energy surface. Furthermore, in chemistry we simplify this problem to 2-dimensions, such that the so-called intrinsic reaction coordinate, or the lowest energy cross section of a higher dimension PES. This yields a reaction coordinate diagram, as is illustrated below in Figure 1.1.

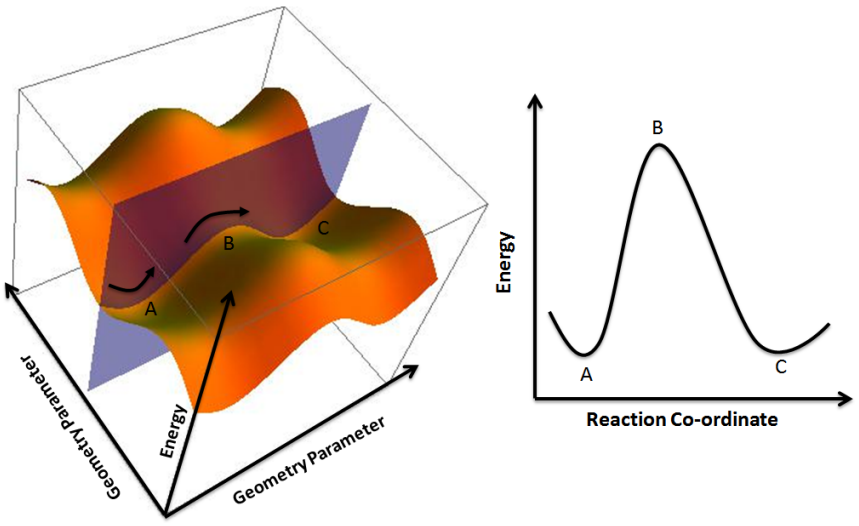

Figure 1.1: Placeholder PES from Wikipedia

In a typical reaction coordinate diagram, the reactants begin to interact and form a pre-reaction complex (A). Given sufficient energy, the reaction will proceed over the top of the energy barrier through a transition state

(TS) complex (B). After the chemical transformation is completed, a post-reaction complex (C) is formed until the products are able to separate.

In quantum chemistry, we are generally not concerned with the dynamics of a chemical reaction, but rather the thermodynamic and kinetic properties of a reaction. This is achieved through the investigation of stationary states (reactants, pre-reaction complex, TS complex, post-reaction complex, and products) along the reaction coordinate. Thermodynamic analysis of a reaction requires the understanding of the stability of the products relative to the reactants, measured by change in Gibbs free energy ΔG, while kinetic analysis requires the understanding of the stability of the TS complex relative to the reactants measured by the Gibbs free energy barrier $\Delta G^{\ddagger}$.(Need to modify figure to include energy)

To fully understand HAT reactions, one must analyse the factors which influence the thermodynamics and kinetics of these reactions. Thermodynamically this is relatively simple; the most important factor to consider is relative bond strengths. Typically, a reaction will be exergonic if the bond being formed is stronger than the bond being broken. Entropic changes (ΔS) in HAT reactions are in all but the most unusual cases, negligible ($\Delta S \approx 0$).[28] Kinetic analysis can be considerably more complicated, as there are numerous factors which can stabilise or destabilise the reactants or TS complex. The important factors include solvent interactions, non-covalent interactions, bond strengths, and stereo-electronic interactions, each of which is described below.

1.2.2 Factors influencing the kinetics of HAT reactions

Solvent interactions

Kinetic solvent effects (KSEs) describe the effect on a reaction from solvent interactions. Solvent has the ability to stabilise or destabilise the TS complex of a HAT reaction. Since the earliest studies describing KSEs in 1964,[29] a great deal of literature exists describing KSEs, especially for HAT reactions involving phenols.[30] Hydrogen bond (HB) formation between phenols and HB accepting solvents is attributed to the observation that increasing solvent polarity decreases the rate constants for HAT reactions (k_H). Unlike phenols, our amide models possess an HB accepting moiety, and thus interact strongly with HB donating solvents. Experimental work from our colleagues in Rome has demonstrated that for C-H bond HAT from substrates with HB accepting capabilities, k_H decreases with solvent HB donating ability. Evidence for this is summarized in Table 1.1: for HAT

reactions of CumO$^{\bullet}$with N,N-dimethylformamide (DMF), tetrahydrofuran (THF), and triethylamine (TEA), as the polarity and HB donating ability of the solvent increases, the rate constant k_H, decreases.

Table 1.1: Second-order rate constants (k_H, $M^{-1}s^{-1}$) for HAT from C-H bonds of hydrogen bond accepting substrates to the cumyloxyl radical measured in different solvents at 25 °C. [a]Reference 31. [b]Reference 32 and 33. [c]Reference 34.

Solvent	N,N-dimethylformamide[a]	Tetrahydrofuran[b]	Triethylamine[c]
isooctane	$(7.7 \pm 0.1) \times 10^6$	$(1.21 \pm 0.02) \times 10^7$	$(2.9 \pm 0.1) \times 10^8$
benzene	$(3.1 \pm 0.1) \times 10^6$	$(7.2 \pm 0.7) \times 10^6$	$(2.8 \pm 0.1) \times 10^8$
MeCN	$(1.24 \pm 0.02) \times 10^6$	$(5.8 \pm 0.2) \times 10^6$	$(2.0 \pm 0.1) \times 10^8$
t-BuOH	$(1.38 \pm 0.03) \times 10^6$	$(5.8 \pm 0.2) \times 10^6$	$(1.61 \pm 0.03) \times 10^8$
MeOH	$(9.8 \pm 0.2) \times 10^5$	$(4.9 \pm 0.2) \times 10^6$	$(3.8 \pm 0.1) \times 10^6$
TFE	$< 1 \times 10^4$	$(2.7 \pm 0.1) \times 10^6$	

The KSEs observed in Table 1.1 can been explained on the basis of hyperconjugation, the donation of electron density from neighbouring orbitals into C-H σ^* antibonding orbitals. Hyperconjugation has a net stabilising effect, however it decreases the strength of C-H bonds by accepting electron density into a C-H σ^* orbital. For the species listed in Table 1.1, abstraction occurs primarily from C-H bonds adjacent to a heteroatom or π system. Hyperconjugative overlap between the heteroatom and C-H σ^* antibonding orbitals in these species is decreased by the formation of a hydrogen bond with solvent, effectively increasing the strength of the C-H bond and thus destabilising the TS complex and increasing $\Delta G^{\ddagger}$. This is the key kinetic effect of solvation in the our model systems.

Non-covalent interactions

Non-covalent interactions (NCIs; eg. van der Waals interactions, hydrogen bonding, etc.) play a central role in all chemistry. It has already been demonstrated that HB formation between substrates and solvents plays an important role, however oxygen centres can also hydrogen bond with substrates as both acceptors and donors.[35] These hydrogen bonding interactions, in addition to the other non-covalent interactions between the radical and substrate lead to the formation of a pre-reaction complex. No literature currently exists which discusses how the strengths of these interactions impacts the kinetics of a reaction, however these effects cannot be ignored. Chapter 4 of this thesis shall deal with this specifically.

Non-covalent interactions are known to be important in the stabilisation of TS complexes in HAT reactions.[36,37] Although the effects of NCI stabilisation are difficult to quantify, the concept of TS complex stabilisation is being recognised in applications such as enzyme catalysis[38] and synthetic catalysis.[39]

It has been demonstrated that the formation of pre-reaction complexes can in fact be the rate-limiting step of a reaction.[40–42] Combined experimental and computational examinations of HAT reactions between the cumyloxyl (CumO$^\bullet$) or benzyloxyl (BnO$^\bullet$) radicals with tertiary alkylamines and alkylamides demonstrated that the relatively acidic α-C-H of BnO$^\bullet$is capable of forming hydrogen bonds with enthalpies (ΔH) of 4.0 kcal mol^{-1} for alkylamines to 8.5 kcal mol^{-1} in alkylamides. The comparison of k_H for these HAT reactions between CumO$^\bullet$and BnO$^\bullet$(k_H^{BnO}/k_H^{CumO}) demonstrates large rate enhancements, ranging from 2.8 for the very sterically hindered triisobutylamine, to 1094 for 1,4-diazabicyclo[2.2.2]octane. In this case, NCIs control the kinetics of the reaction not through stabilisation, but rather through changing the rate-determining step.

Bond strengths and the Bell-Evans-Polanyi Principle

It has long been the interest of chemists to understand chemical reactions from both a thermodynamic and kinetic standpoint. The measurement and comparison of bond strengths, that is bond dissociation enthalpies (BDEs), is central to the understanding of reactivity with respect to thermodynamics. There exists a tremendous amount of literature in which BDEs are linked to chemical reactivity, especially for HAT reactions.[1,43–46]

Often, BDEs are used in linear free energy relationships (LFERs) to relate chemical reactivity to bond strength. One such example[45] is the application of BDEs to the Hammett equation,[47] which can be used to study substituent effects from thermodynamic (Equation 1.4) or kinetic analysis (Equation 1.5).

$$\log \frac{K_X}{K_H} = \rho\sigma_X \tag{1.4}$$

$$\log \frac{k_X}{k_H} = \rho\sigma_X \tag{1.5}$$

In the above equations, K is an equilibrium constant and k is a rate constant for either a reference reaction with a hydrogen substituent H or a given substituent X. The substituent parameters σ_X, have been measured

for various different reference reactions, although the original parameters were measured for the acidity of benzoic acid.[48] Plots of $\log(K_X/K_H)$ or $\log(k_X/k_H)$ against σ_x have been used to determine ρ, the sensitivity constant. Originally ρ was used to determine whether a reaction was more sensitive ($\rho > 1$), less sensitive ($\rho < 1$), or equally sensitive to substituents than benzoic acid, with negative charges being produced. If ρ is negative then positive charge is said to be formed as a result of substituents.

In the context of BDEs, Pratt et al.[45] examined a series of substituents (Y) on toluenes, anilines, and phenols (4-YC_6H_4−ZX), and showed that the Z-X BDEs can be correlated to the electrophilic substituent constants, $\sigma_p^+(Y)$. This was surprising because it demonstrated that homolytic properties correlated with properties derived from the heterolytic S_N1 solvolyses of para-substituted cumyl chlorides.[49] Specifically, this showed that since $\sigma_p^+(Y)$ describes the relative ability of Y to stabilise a positive charge, the ability to stabilise strong electron withdrawing (EW) moieties can be well described in general by these parameters. This means that BDEs for toluenes and anilines are well correlated to $\sigma_p^+(Y)$, since $O^\bullet$ and $NH^\bullet$ can be described like positive charges (strong EW groups). Toluenes, which have resulting radicals ($CH_2^\bullet$) which are neither electron withdrawing nor donating, are poorly correlated with $\sigma_p^+(Y)$.

Another interesting LFER, which is utilised in Chapter 5, is the Bell-Evans-Polanyi (BEP) Principle,[50,51] which states that the difference in activation energy (E_a) for two related reactions (within the same family), is proportional to the differences in reaction enthalpy (ΔH):

$$E_a = E_0 + \alpha \Delta H \tag{1.6}$$

This relationship has been more generally used to compare larger families of reactions. The remaining terms in Equation 1.6 are E_0, the activation energy of a reference reaction, and α is a constant which characterises the position of the TS along the reaction coordinate. This can be rationalised by considering a series of reactions with similar energy profiles: if the reaction becomes more exothermic, the barrier height will decrease (the opposite is also true for endothermic reactions), as illustrated in Figure 1.2.

If the BEP relationship holds for a series of related HAT reactions, then BDEs should correlate with the activation energy, where increased bond strengths would represent a destabilisation in the TS complex. In practice, plots of BDEs against the logarithm of rate constant are used. An interesting example of this is the work of Pratt et al.[15], in which the free radical

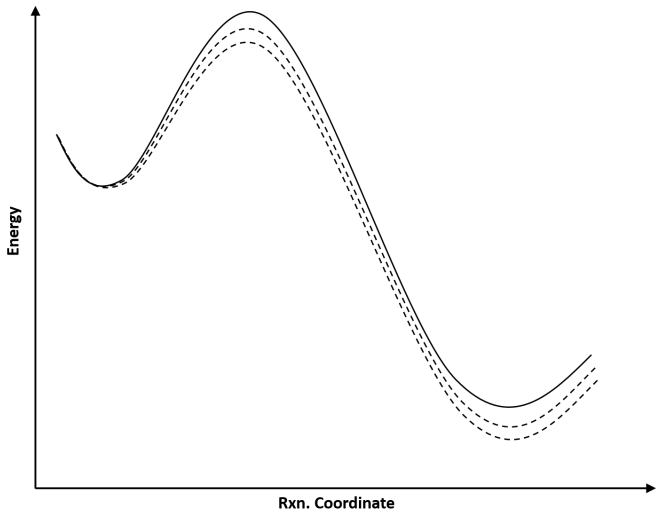

Figure 1.2: Energy profiles for a series of related exothermic reactions illustrating the Bell-Evans-Polanyi Principle.

oxidation of unsaturated lipids is examined. They achieve this through the correlation of theoretically determined C-H and C−OO$^\bullet$ bond strengths with experimentally measured HAT rate constants and O_2 addition rate constants, respectively. BEP plots (BDE vs. $\log k$) for a large range of polyunsaturated fatty acid models show good correlation for both the C-H bonds and C−OO$^\bullet$ bonds examined. This demonstrates that BDEs have a direct impact on the reaction barrier height, giving validation to the BEP Principle.

Although chemists often consider the importance of BDE in thermodynamic analysis, bond strengths are an important consideration in kinetic analysis as well. As such, the altering of bond strengths can be an important factor in related HAT reactions. The generallity of application of the BEP Principle is discussed in Chapter 5.

Stereo-Electronic interactions

The effects of sterics and electronics have been shown to play an important role in HAT reactions. Generally, these effects are described as two seperate phenomena: polar effects and steric effects.

The species involved in HAT reactions are often neutral radicals, thus the influence of charge transfer in the TS complex can have important im-

plications. Consider the TS of a generic HAT reaction in Scheme 1.3, there are four obvious resonance forms. For a series of related reactions, E_a would be expected to decrease as the contribution of dipolar ion resonance forms increases.[52] Oxygen centred radicals are electrophilic in nature, thus the importance of the third resonance structure becomes important. HAT is favoured from C-H bonds which are electron rich, or nucleophilic.[53]

$$\left[\mathrm{X\text{–}H\text{–}Y}\right]^{\ddagger}$$

$$[\mathrm{X^{\bullet}H{-}Y}]^{\ddagger} \longleftrightarrow [\mathrm{X{-}HY^{\bullet}}]^{\ddagger} \longleftrightarrow [\mathrm{X{:}^{-}H^{\bullet}Y^{+}}]^{\ddagger} \longleftrightarrow [\mathrm{X^{+}H^{\bullet}Y{:}^{-}}]^{\ddagger}$$

Scheme 1.3: A generic HAT transition state structures and possible resonance forms.

An example of this effect is from the work of our colleagues in Rome,[33,54] in which rate constants (k_H, normalised for the number of abstractable hydrogens) for cyclohexane and acetone to the cumyloxyl radical (CumO$^{\bullet}$) were measured and compared to theoretically determined C-H BDEs. Cyclohexane has a C-H BDE = 99.5 kcal mol^{-1} and $k_H = 9.2 \times 10^4$ M^{-1}s^{-1} , while acetone has C-H BDE of 96.0 kcal mol^{-1} and $k_H = < 2 \times 10^3$ M^{-1}s^{-1} . As a result of polar effects, although cyclohexane has a greater bond strength, it is at least an order of magnitude more reactive in HAT than acetone.

The effects of steric bulk also play an important role in HAT, and have been studied extensively by our colleagues in Rome, as well as by others.[33,40,54–59] Although a C-H bond may be weaker than others on a given substrate, if it is not accessible due to steric constraints, abstraction will not occur at this site. Otherwise, additional steric bulk can lead to significant reductions in reactivity, through destabilisation of the TS complex. For example, in reactions of tertiary acetamides with CumO$^{\bullet}$,[59] where abstraction occurs mainly from C-H bonds α to the nitrogen atom, a two fold decrease in normalised rate constant is observed in going from N,N-dimethylacetamide to N,N-diisobutylacetamide ($k_H = 2.0 \times 10^5$ and 7.8×10^4 M^{-1}s^{-1} , respectively).

1.2.3 Mechanistic details of hydrogen transfer reactions

For a simple HAT reaction, as shown in Scheme 1.4, there exists several possible mechanisms by which this transformation can occur. The two most common concerted mechanisms are direct HAT[60] and proton-coupled electron transfer (PCET). At the basic level, direct HAT involves the transfer

of an electron and proton through the same set of acceptor/donor orbitals, while PCET involves the transfer of an electron and proton through different sets of orbitals. In practise, this distinction is poorly described and this topic is still in active discussion in the literature.[37,46,61–69] Primarily, the distinction between the two processes is unclear because the two processes cannot be entirely separated physically.[37]

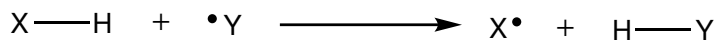

Scheme 1.4: A generic formal hydrogen transfer reaction.

The quintessential example when comparing direct HAT to PCET is the self-exchange reactions of benzyl/toluene and phenoxyl/phenol shown in Scheme 1.5, as described by Mayer et al.[62].

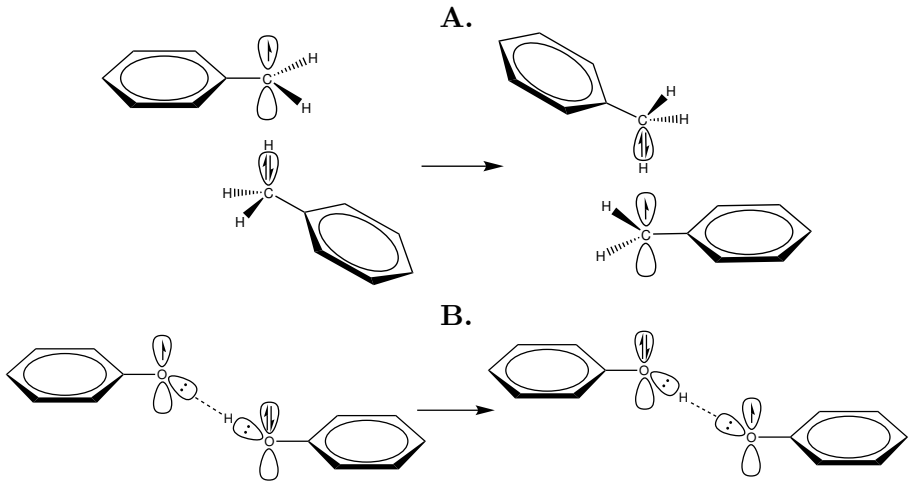

Scheme 1.5: Self-exchange reactions of the **A.** benzyl/toluene couple through direct HAT **B.** phenoxyl/phenol couple through PCET.

In this work, the transition state structures, obtained through theoretical studies, were reported. The proposed structures have C_{2h} and C_2 symmetry for Scheme 1.5 A and B, respectively, oriented so that the aromatic rings are trans relative to one another. In this geometry, the benzyl/toluene pair undergoes direct HAT, with the $2p-\pi$ orbital of the benzylic carbon radical oriented at the benzylic hydrogen on toluene and little delocalisation of

the radical into the π-system. Additionally, the singly occupied molecular orbital (SOMO) is of σ symmetry. The calculated enthalpic barrier ($\Delta H^{\ddagger}$) is 17.7 kcal mol^{-1} . For the phenoxyl/phenol pair, a fairly strongly hydrogen bonded pre-reaction complex is first formed (-8.1 kcal mol^{-1} , relative to reactants). The TS structure is such that the phenoxyl radical occupies a $2p$ orbital, and is allowed to overlap with the $2p$ lone pair of the phenol moiety and the aromatic π systems. This demonstates that the SOMO is of π symmetry and highly delocalised, and that HAT occurs through a PCET mechanism. The reaction has a barrier height $\Delta H^{\ddagger} = 5.0$ kcal mol^{-1} relative to the hydrogen bonded complex, so that the barrier is 3.1 kcal mol^{-1} below the separated reactants.

The work by Mayer et al.[62] suggests that hydrogen bonding is a necessary, but not sufficient condition for PCET to occur. This then implies that PCET is not possible between molecules which do not possess hydrogen bonding moeities, such as carbon atoms. Work by other authors has shown this to be untrue.[37,70] In particular, DiLabio and Johnson[37] demonstrated that this neglected the important contributions of $\pi - \pi$ interactions and lone pair-π interactions. Additional calculations revealed there exists a TS structure for the benzyl/toluene couple which is 3.7 kcal mol^{-1} lower in energy than previously reported. This structure has C_2 symmetry with the aromatic rings oriented 34° relative to one another, allowing for optimal π-stacking, and thus π-π overlap opens up an electronic channel for PCET to occur. They also suggest that the phenol/phenoxyl couple likely prefers a π-stacked TS structure, and compare this to a structural analogue, a naturally occuring tyrosyl/tyrosine couple. Additional work by Muñoz-Rugeles et al.[69] confirmed the existance of a π-stacked TS structure for the phenol/phenoxyl couple. They used an approach which utilises natural population analysis along the intrinsic reaction coordinate, and demonstrated that both the benzyl/toluene couple and phenoxyl/phenol couple favour a π-stacked TS structure and undergo HAT through a PCET mechanism. Interestingly, they also showed that reaction barrier heights for the PCET mechanism are systematically lower than those for direct HAT.

As there is not an obvious way to explore the differences in mechanism experimentally, computational examination of formal HAT reactions enables analysis of the mechanism of these reactions. Using a variety of tools, a general distinction between a HAT mechanism and PCET mechanism can be achieved, however, as stated previously, these mechanisms are not mutually exclusive. Regardless, important insight can be gained from understanding the electronic behaviour of these reactions.

1.2.4 The effects of metal cations on HAT reactions

Solvent interactions in HAT reactions can be described as Lewis acid/base interactions. In biological systems, the most common solvent is water, which can act as both a Lewis acid and base, due to its self-ionising equilibrium. Other important Lewis acids in biology are the non-redox active alkali and alkaline earth metal cations that are present ubiquitously throughout biological systems. Metal ions such as sodium, magnesium, potassium, and calcium are essential to biological function.[71] (Include something about number of ions per protein and/or biological concentrations)

Given the Lewis acid/base nature of these non-redox active metals, we were driven to explore the effects upon HAT reactions. Experimental investigation of these effects has been underway by the Bietti group in Rome. The effects of non-redox active metal cations on HAT from C-H bonds of cyclohexadiene (CHD), tetrahydrofuran (THF), and tertiary alkylamines to CumO$^{\bullet}$were examined.[72] This work is summarized in Table 1.2. Additional experiments examining the same reactions of *N*, *N*-dimethylacetamide (DMA) and *N*, *N*-dimethylformamide (DMF),[31] as well as for various other acetylamides[73] have been performed, and provides the experimental background for this thesis.

In general, metal cation interactions lead to deactivation of C-H bonds and experimental rate constants decrease as a result. An explaination for this is the same as for KSEs, where Lewis acid binding causes a decrease in α-C-H bond σ^* population, thus increasing the effective C-H bond strength and decreasing k_H. For cyclohexadiene, a marginal increase in k_H was observed with additions of 1.0 M $LiClO_4$ and $Mg(ClO_4)_2$, which was explained on the basis of interactions of the metals with CumO$^{\bullet}$. This demonstrates that metal cations have a limited ability to influence HAT reactions of CumO$^{\bullet}$with alkene based substrates. For THF, k_H is 2.0 and 3.2 times lower with the addition of 1.0 M $LiClO_4$ and $Mg(ClO_4)_2$, respectively. $LiClO_4$ has a roughly 2-fold decreasing effect on k_H for alkylamines, whereas $Mg(ClO_4)_2$ has a significantly greater effect, decreasing k_H by more than two orders of magnitude, an effect that has been attributed to the compact charge density of Mg^{2+}. As a whole, these results suggest that metal ions interact more strongly with substrates than CumO$^{\bullet}$, thus C-H bond deactivation is observed due to Lewis acid/base effect. The Lewis acidity of the metal appears to have an important role, since $Mg(ClO_4)_2 > LiClO_4$ in regards to Lewis acidity and effect on k_H. The Lewis basicity of the substrate is also clearly important. Alkylamines undergo a larger decrease in k_H, relative to THF, as they are stronger Lewis bases. Computational studies have

Table 1.2: Summary of experimental rate constants of HAT with CumO$^{\bullet}$ for cyclohexadiene (CHD), tetrahyrofuran (THF), triethylamine (TEA), and 1,2,2,6,6-pentamethylpiperidine (PMP), including the effect of non-redox active metal cations. Rate constants were determined by LFP in 25 °C MeCN. *Rate constants are approximate as the effects of even small additions of metal cations cause rate outside the range of laser flash photolysis experiments.

Substrate	Conditions	$k_H(\mathrm{M}^{-1}\mathrm{s}^{-1})$
CHD		$(6.65 \pm 0.02) \times 10^7$
	$LiClO_4$ 1.0 M	$(7.49 \pm 0.04) \times 10^7$
	$Mg(ClO_4)_2$ 1.0 M	$(7.0 \pm 0.1) \times 10^7$
THF		$(5.7 \pm 0.1) \times 10^6$
	$LiClO_4$ 1.0 M	$(2.87 \pm 0.04) \times 10^6$
	LiOTf 1.0 M	$(2.8 \pm 0.2) \times 10^6$
	$Mg(ClO_4)_2$ 1.0 M	$(1.8\pm 0.1) \times 10^6$
TEA		$(2.0 \pm 0.1) \times 10^8$
	$LiClO_4$ 1.0 M	$(9.37 \pm 0.01) \times 10^7$
	$Mg(ClO_4)_2$ 0.005 M	$< 1 \times 10^{6*}$
PMP		$(1.70 \pm 0.02) \times 10^8$
	$LiClO_4$ 1.0 M	$(9.0 \pm 0.3) \times 10^7$
	$Mg(ClO_4)_2$ 0.005 M	$< 1 \times 10^{6*}$

validated these results, demonstrating that binding of $Mg(ClO_4)_2$ leads to a 5.1 kcal mol^{-1} decrease in the α-C-H BDE in TEA and that k_H decreases by > 4 orders of magnitude.[74]

Simple amides such as DMF and DMA are often used as simple peptide models.[75] As such the deactivation of C-H bonds in amides, as indicated by the observed decreases in k_H, leads to the central hypothesis of this thesis: *non-redox active metals cations can serve as chemoprotective agents for biomolecules*. Experimental evidence for this is demonstrated in Figure 1.3. For $LiClO_4$ added to DMF and DMA, total inhibition of HAT occurs up to 2 and 1 molar equivalents, respectively. Inhibition of HAT occurs for 2 and 4 molar equivalents, respectively, followed by total non-inhibition. A much weaker effect is observed with $NaClO_4$, while a similar strong deactivating effect is observed for $Ca(ClO_4)_2$. The addition of $Mg(ClO_4)_2$ gives weak deactivation for the first two molar equivalents of both DMF and DMA, with strong activation for an additional two equivalents. This unusual behaviour is as of yet, unexplained. Additional discussion of experimental results shall be reserved for Chapter 6.

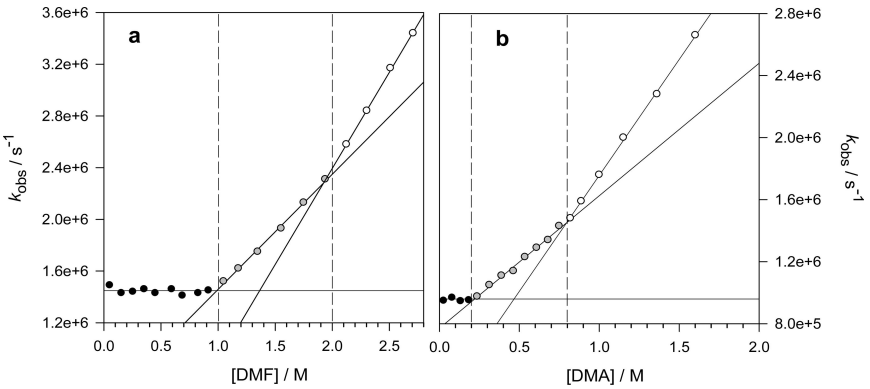

Figure 1.3: Plots of observed rate constants against concentation of substrate for HAT reactions with cumyloxyl radical: **a** Substrate = DMF, measured by LFP at 25°C in solutions of MeCN containing 1.0 M dicumyl peroxide and 0.5 M $LiClO_4$. Complete inhibition of HAT is observed at 0-1.0 M, while linear regression for the 1.0-2.0 M regions gives $k_{H1} = 8.91 \times 10^5$ $M^{-1}s^{-1}$, and $k_{H2} = 1.49$ [6] $M^{-1}s^{-1}$ in the 2.0-2.7 M region. **b** Substrate = DMA, measured by LFP at 25 °C in solutions of MeCN containing 1.0 M dicumyl peroxide and 0.2 M $LiClO_4$. Complete inhibition of HAT is observed at 0-0.2 M, while linear regression in the 0.2-0.8 M region gives k_{H1}=8.54 $\times 10^5$ $M^{-1}s^{-1}$ and $k_{H2} = 1.49 \times 10^6$ $M^{-1}s^{-1}$ in the 0.8-1.6 M region. Figure taken from Reference 31.

Chapter 2

Theory

2.1 The quantum mechanical approach

In quantum chemistry we seek solutions to the non-relativistic time-independent Schrödinger equation

$$\mathscr{H} |\Psi\rangle = E |\Psi\rangle \tag{2.1}$$

where $\mathscr{H}$ is the Hamiltonian operator for a system of nuclei and electrons, and Ψ are the set of eigenvectors with energy eigenvalues E.[76] For a system with N electrons and M nuclei, the full Hamiltonian in atomic units is

$$\begin{aligned} \mathscr{H} = &- \sum_{i=1}^{N} \frac{1}{2} \nabla_i^2 - \sum_{A=1}^{M} \frac{1}{2M_A} \nabla_A^2 - \sum_{i=1}^{M} \sum_{A=1}^{M} \frac{Z_A}{r_{iA}} \\ &+ \sum_{i=1}^{N} \sum_{j>i}^{N} \frac{1}{r_{ij}} + \sum_{A=1}^{M} \sum_{B>A}^{M} \frac{Z_A Z_B}{R_{AB}} \end{aligned} \tag{2.2}$$

In this equation, Z_A is the atomic number of nucleus A with a mass M_A divided by the mass of an electron. The Laplacian operators ∇_i^2 and ∇_A^2 represent differentiation with respect to the coordinates of the ith electron and Ath nucleus. The first and second terms are the kinetic energies of the electrons and nuclei, respectively. The third term represents the Coulomb attraction between electrons and nuclei with distance r_{iA}. The fourth and fifth terms represent repulsion between two electrons with distance r_{ij}, and between two nuclei with distance R_{AB}, respectively.

Nuclei move slowly relative to electrons, due to their much greater mass. This is the central pillar of the Born-Oppenheimer approximation that is nearly always applied in molecular electronic structure calculations. The application of this approximation allows for the simplification of Equation 2.2 by neglecting the second term for nuclear kinetic energy, and assuming the last term of nuclear repulsion is constant, and thus can also be ignored. This leaves us with the electronic Hamiltonian

$$\mathscr{H}_{elec} = -\sum_{i=1}^{N} \frac{1}{2}\nabla_i^2 - \sum_{i=1}^{M}\sum_{A=1}^{M} \frac{Z_A}{r_{iA}} + \sum_{i=1}^{N}\sum_{j>i}^{N} \frac{1}{r_{ij}} \tag{2.3}$$

Unfortunately, it is only possible to exactly solve the Schrödinger equation for the full electronic Hamiltonian $\mathscr{H}_{elec}$ in the simplest of cases: when there is only one electron (H, H_2^+, He^+, Li^{2+}, etc). Note that since we will always work within the Born-Oppenheimer approximation, the subscript *elec* is usually dropped. In order to proceed to systems with multiple electrons, we must make further approximations.

2.1.1 Spin and Spatial Orbitals

We will refer to the wave function of a single particle as an orbital. Naturally then, as we will deal with electrons in molecules, we shall refer to their wave functions as molecular orbitals (MOs). To fully describe electrons we must consider a spatial and spin component to the overall wave function. A spatial orbital $\psi_i(\mathbf{r})$, is a function of the position vector $\mathbf{r}$, and describes the distribution of an electron in all space. It is usually assumed that spatial MOs form an orthonormal set such that

$$\langle \psi_i(\mathbf{r}) | \psi_j(\mathbf{r}) \rangle = \int d\mathbf{r} \psi_i^*(\mathbf{r}) \psi_j(\mathbf{r}) = \delta_{ij} \tag{2.4}$$

where the left-hand side is standard Dirac *bra-ket* notation representing the same integral in the middle. The right-hand side of Equation 2.4 is the standard Kronecker delta.

The spin of an electron is represented by two orthonormal functions $\alpha(\omega)$ and $\beta(\omega)$, or spin up and spin down. If a wave function describes both the spatial distribution and spin of an electron it is a spin orbital, $\chi_i(\mathbf{r})$, where $\mathbf{x}$ represents both the spatial distribution and spin coordination of an electron ($\mathbf{x} = \{\mathbf{r}, \omega\}$). Since $\psi_i(\mathbf{r})$ and $\alpha(\omega)/\beta(\omega)$ are orthonormal, so too is $\chi_i(\mathbf{x})$

$$\langle \chi_i(\mathbf{x}) | \chi_j(\mathbf{x}) \rangle = \delta_{ij} \tag{2.5}$$

2.1.2 The Hartree product

The first steps towards describing an N electron wave function come from the work in the late 1920s by Hartree. The early *Hartree method* took an approach in which the wave function of N non-interacting electrons (Ψ^{HP}) is described by the product of N spin orbitals, known as a *Hartree product*:

$$\Psi^{HP}(\mathbf{x}_1, \mathbf{x}_2, \ldots, \mathbf{x}_N) = \chi_i(\mathbf{x}_1)\chi_j(\mathbf{x}_2)\ldots\chi_k(\mathbf{x}_N) \tag{2.6}$$

In such a system the Hamiltonian has the form of a sum of N independent operators, each decribing an electron's kinetic and potential energy ($h(i)$):

$$\mathscr{H} = \sum_{i=1}^{N} h(i) \tag{2.7}$$

Solutions to the Schrödinger equation for this system of non-interacting electrons are facile to obtain as each $h(i)$ depends only on the variables of $\chi_i(\mathbf{x}_i)$, so that

$$\mathscr{H}\left|\Psi^{HP}\right\rangle = E\left|\Psi^{HP}\right\rangle \tag{2.8}$$

gives an eigenvalue energy solution E that is the sum of N spin orbital energies ε_i

$$E = \varepsilon_1 + \varepsilon_2 + \cdots + \varepsilon_N \tag{2.9}$$

While this theory does allow one to calculate energies for an N electron system, it has a basic deficiency: it does not follow the antisymmetry principle of wave functions. The antisymmetry principle states that the electronic wave function must change sign (be antisymmetric) with respect to the exchange of spacial and spin coordinate of any two electrons. Hartree accounted for this by nominally applying the Pauli exclusion principle, however, this description is still incomplete in the sense that it does not describe the statistical nature of quantum particles.

2.1.3 Slater determinants

In order to satisfy the antisymmetry principle, a linear combination of Hartree products can be taken. Although the method was first utilised independently by Heisenberg[77] and Dirac,[78] this method is called a *Slater determinant* after Slater.[79] For an N electron system, a Slater determinant is written as

$$\Psi(\mathbf{x_1}, \ldots, \mathbf{x_N}) = \frac{1}{\sqrt{N!}}\begin{vmatrix} \chi_i(\mathbf{x}_1) & \chi_j(\mathbf{x}_1) & \ldots & \chi_k(\mathbf{x}_1) \\ \chi_i(\mathbf{x}_2) & \chi_j(\mathbf{x}_2) & \ldots & \chi_k(\mathbf{x}_2) \\ \vdots & \vdots & \ddots & \vdots \\ \chi_i(\mathbf{x}_N) & \chi_j(\mathbf{x}_N) & \ldots & \chi_k(\mathbf{x}_N) \end{vmatrix} \tag{2.10}$$

where $1/\sqrt{(N!)}$ is a normalisation factor. This simple mathematical trick ensures antisymmetry since the interchange of two electrons requires the exchange of two rows in the determinant, which changes the sign. Normally the short-hand form, which implicitly includes the normalisation factor and assumes the ordering of electrons is $\mathbf{x}_1, \mathbf{x}_2, \ldots, \mathbf{x}_N$, is written as only the diagonal elements of the determinant:

$$\Psi(\mathbf{x}_1, \mathbf{x}_2, \ldots, \mathbf{x}_N) = |\chi_i \chi_j \cdots \chi_k\rangle \tag{2.11}$$

Slater determinants are completely dependent on the spin orbitals from which it is formed, to within a sign. Therefore, Slater determinants also form an orthonormal set. Additionally, the introduction of antisymmetry into the Hartree product incorporates so-called *exchange correlation*. This means that the motion of two electrons with parallel spin are correlated. However, since the motion of electrons with opposite spin are not correlated, a single determinant wave function is said to be uncorrelated.

2.1.4 The Hartree-Fock approximation

Now that we have a method for describing many-electron wave functions, we can consider the computation of molecular properties. The cornerstone of quantum chemistry is the *Hartree-Fock method* (HF), otherwise known as the self-consistent field method. The main principle of the HF method is to approximate electron-electron interactions with an average potential. We begin with a single Slater determinant for an N electron system in the ground state:

$$|\Psi_0\rangle = |\chi_1 \chi_2 \cdots \chi_N\rangle \tag{2.12}$$

By applying the variational method to the Schrödinger equation, we hope to find the lowest possible energy

$$E_0 = \langle \Psi_0 | \, \mathscr{H} \, | \Psi_0 \rangle \tag{2.13}$$

Within the Hartree-Fock approximation, we approximate the full electronic Hamiltonian $\mathscr{H}$ with a related operator $\hat{H}_0$:

$$\hat{H}_0 = \sum_{i=1}^{N} \hat{f}(i) \tag{2.14}$$

where $\hat{f}(i)$ is the Fock operator of the ith electron. The problem is now reduced to solving the eigenvalue Hartree-Fock equation of the form

$$\hat{f}(i)\chi(\mathbf{x}_i) = \epsilon_i\chi(\mathbf{x}_i) \tag{2.15}$$

Solving Equation 2.15 directly is computationally very challenging, as there are infinite possible solutions. However in 1951, Roothaan [80] demonstrated that the problem can be simplified by expanding each spin orbital into a linear combination of a known finite number K basis functions:

$$\chi_i = \sum_{\mu=1}^{K} C_{\mu,i}\phi_\mu \tag{2.16}$$

where $C_{\mu,i}$ is a weighting coefficient and ϕ_μ is a basis function. As K approaches ∞, the set $\{\phi_\mu\}$ becomes more complete and the energy approaches the so-called *Hartree-Fock limit*, or the exact energy in the Hartree-Fock approximation. One is however always limited to a finite number of basis functions, leaving deficiencies in the desired wave function Ψ_0.

The expansion of spin orbitals into a basis allows Equation 2.15 to be written in terms of the *Roothaan matrix equation*

$$\mathbf{FC} = \mathbf{SC}\varepsilon \tag{2.17}$$

where $\mathbf{F}$ is the Fock matrix, $\mathbf{S}$ is the orbital overlap matrix, $\mathbf{C}$ is the orbital coefficient matrix, and ε is the diagonal matrix of orbital energies ε_i. By performing a transformation of basis such that the overlap matrix $\mathbf{S}$ becomes the identity matrix $\mathbb{1}$, the problem becomes a matter of diagonalising $\mathbf{F}$. This must be done iteratively, as $\mathbf{F}$ depends on its own solution, hence the name self-consistent field method.

2.1.5 Basis sets

Choosing optimal basis functions can help significantly in terms of determining the ground state wave function Ψ_0. Quantum chemists rely on the choice of *basis sets*, defined as the vector space in which an *ab initio* problem is defined. Basis sets usually refer to the set of one particle functions, which are used to form MOs in a linear combination of atomic orbitals (LCAO-MO) like approach. For a system with N electrons, the LCAO-MO approach gives $N/2$ occupied orbitals in the ground state. The remaining basis functions in a set are combined to give *virtual* (unoccupied) orbitals.

Early basis sets were composed of *Slater-type orbitals* (STOs), due to their resemblance to the atom orbitals (AOs) of the hydrogen atom. These are functions of the form

$$\phi_i^{STO}(\zeta, n, a, b, c, x, y, z) = Nr^{n-1}e^{-\zeta r}x^a y^b z^c \tag{2.18}$$

where N is a normalisation constant, ζ is a constant related to the effective nuclear charge of the nucleus, r is the distance of the electron from the atomic nucleus, n is a natural number that plays the role of the principle quantum number, and x, y, and z are cartesian coordinates. The angular component $x^a y^b z^c$ describes the shape of the orbital, such that if a+b+c=0 ϕ_i^{STO} is of s-type; if $a+b+c=1$, ϕ_i^{GTO} is of p-type, and so forth. Although STOs approximate the long and short range behaviour of atomic orbitals correctly, performing integration with these functions is computationally very expensive.

In modern quantum chemistry, basis sets are almost exclusively composed of *Gaussian-type orbitals* (GTOs), which can generally be represented as

$$\phi_i^{GTO}(\alpha, a, b, c, x, y, z) = Ne^{-\alpha r^2}x^a y^b z^c \tag{2.19}$$

where N is a normalisation constant, α is the orbital exponent coefficient, x, y, and z are cartesian coordinates, r is the radius ($r^2 = x^2 + y^2 + z^2$), and the angular portion is described the same as in an STO. It takes a linear combination of several GTOs to represent the same function as an STO. These linear combinations of GTOS are known as *contracted GTOs* (CGTO) with n GTOs combined as

$$\phi_i^{CTGO}(\alpha, a, b, c, x, y, z) = N\sum_{i=1}^{n} c_i e^{-\alpha r^2}x^a y^b z^c \tag{2.20}$$

where c_i is referred to as the contraction coefficient which describes the weighting of each GTO. Although it requires more GTOs than STOs to accurately describe the atomic orbitals, the integrals can be computed 4-5 times faster, and thus GTOs are much more efficient.[81]

Basis set nomenclature

We now know that standard basis sets are composed of basis functions which represent atomic orbitals and that each basis function is a CGTO composed of several GTOs. A *minimal basis set* is one in which each AO is represented by a single basis function. To more accurately represent AOs, more basis functions should be used, although basis set size needs to be balanced with computational cost. Larger basis sets are referred to by their cardinal number, the number of basis functions which represent each AO.

When two basis functions are used to represent each AO, this is called a *double-zeta* basis set. If three basis functions represent each AO, this is called a *triple-zeta* basis set. Generalised, a basis set is N-zeta in size when N basis functions are used per AO.

A *split-valence* basis set is one in which a single basis function is used to represent each core AO, while more basis functions are used to represent the valence AOs. Constructing basis sets in this way can help reduce the computational cost while still accurately representing the electrons which are most important to chemistry.

Additional basis functions are often added to basis sets in order to correctly describe molecular properties. *Polarisation functions* are basis functions which are one or more angular momentum channels greater than the natural electronic configuration of an atom. For example, a single p-type basis function can be added to the minimal basis of a hydrogen atom. Polarisation functions are essential to accurately describe chemical bonding, as the presence of other atoms distorts the spherical symmetry of a single atom's AOs.[82] *Diffuse functions* are basis functions which extend further into space, typically by the inclusion of a very shallow Gaussian function (small ζ exponent). Diffuse functions are necessary to accurately describe anions, very electronegative atoms, and large systems in which NCIs are important.

Commonly used basis sets

A large number of basis sets currently exist in the literature.[83] While not all basis sets are created equally, we shall briefly describe four of the most commonly used basis sets used in quantum chemistry. (I have only included the first citation for the basis sets. Maybe include more.)

Pople-style basis sets

Perhaps the most utilised basis sets in chemistry are those arising from the group of Pople.[84] These basis sets were defined by fitting to HF wave functions. The earliest of these basis sets are the minimal STO-NG basis sets, where N describes the number of GTOs that go into each contraction.

The practise of using minimal basis sets has diminished significantly as technology has advanced, thus these basis sets are largely considered out of date. It is more common to utilise the split-valence basis sets, denoted as $n-ijG$ or $n-ijkG$ for double and triple zeta split-valence basis sets, respectively. In this system of notation, n represents the number of GTOs that comprise the core AOs, and i, j, k describe the number of GTOs for

contractions in the valence AOs. Polarisation functions are denoted either with asterisks or with the specific shell and number of functions which are being added. Diffuse functions are denoted with either a single or double "+", indicating diffuse s and p-type functions for heavy atoms, and the addition of diffuse s-type functions for hydrogen, respectively. For example, the 6-31+G(d,p) $\equiv$ 6-31+G** double-zeta basis set is one which has: 6 GTOs per core AO, 3 GTOs for the first valence set of AOs, and 1 GTO for the second, along with s and p diffuse functions of the heavy atoms, a single d polarisation function of heavy atoms, and a single p polarisation function of hydrogen atoms.

Correlation consistent basis sets

Post-Hartree-Fock methods (*vide infra*) are commonly used in quantum chemistry. In 1989, Dunning[85] identified that the use of basis sets optimised for HF were inappropriate for post-HF methods. The basis sets that came from Dunning and co-workers, which are referred to as "correlation consistent" basis sets are commonly used in, but not limited to, state of the art wave function calculations. Correlation consistent basis sets are denoted as "cc-pVNZ", where N=D,T,Q,5,6,... is the cardinal number of the basis set. These are large sets containing polarisation functions by default and can be additionally augmented with diffuse functions, denoted by "aug." A commonly used basis set is aug-cc-pVTZ, which is a triple-zeta basis set with implicit polarisation functions and specified diffuse functions on all atoms.

Polarisation consistent basis sets

The polarisation consistent basis sets have been developed by Jensen and coworkers.[86] Like the correlation consistent basis sets, the polarisation consistent basis sets have been developed to systematically approach the HF limit, or analogous complete basis set limit in density-functional theory calculations. The notation adopted is "pc-X", where X is the cardinal number of the basis set minus one (i.e. $X = N$-1). Polarisation functions are included by default in these basis sets, and additional diffuse functions can be specified with the same "aug" notation as the correlation consistent basis sets.

Ahlrich basis sets

The last basis sets we will mention are those developed by Ahlrich and coworkers.[87] These are the "Def2" basis sets, named as such because they are the second generation of default basis set in the Turbomole quantum chemistry package.[88] A unique optimisation technique employing the calcu-

lation of gradients of energy with respect to the individual basis function terms was utlised in the development of these set. Addtionally, these basis sets have been developed for nearly every element on the periodic table, which is a unique trait among modern basis sets. The nomenclature for these basis sets is fairly straightforward where either SV is used for split valence, or NZ is used for cardinal number. Addition of polarisation and diffuse functions is specified with a P and D, respectively. For example, Def2-SVP is the basis set of split-valence double-zeta quality with polarisation functions; Def2-TZVP is the triple-zeta basis set with polarisation functions; Def2-QZVPD is the quadruple-zeta basis set with polarisation and diffuse functions.

2.1.6 Post-Hartree-Fock methods

The HF method gives an approximation to the ground state wave function of a molecule for a reasonable computational cost (scaling with N^4 number of basis function). There is however, a lack of the complete description of *dynamical electron correlation*,[89] and thus significant deviations from experimental results can be observed. Dynamical electron correlation is a measure of how much one electron's movement is affected by the presence of other electrons. As described previously, the HF method includes the correlation of the movement of electrons with the same spin through the exchange interactions included by using a Slater determinant, however other correlation effects are also important and must be included to obtain accurate results. The majority of methods take the HF wave function Ψ_0 as the starting point. Normally, the total energy is obtained by addition of an energy correction for correlation E_{corr}, which can be defined as

$$E_{corr} = \Xi_{tot} - E_0 \tag{2.21}$$

where Ξ_{tot} is the full non-relativistic energy from the Schrödinger equation and E_0 is the reference state energy, usually the HF energy.

We shall briefly describe two important methods for accounting for electron correlation and obtaining E_{corr}: Møller-Plesset perturbation theory, and the related configuration interaction and coupled cluster theories.

Møller-Plesset perturbation theory

Møller-Plesset (MP) perturbation theory is a special case of Rayleigh-Schödinger perturbation theory in which the Hamiltonian for a system can be approximated by

$$\hat{H} = \hat{H}_0 + \lambda \hat{V} \tag{2.22}$$

where $\hat{H}_0$ is an unperturbed Hamiltonian, $\hat{V}$ is a small perturbation, and λ is an arbitrary parameter which controls the size of the perturbation. The perturbed wave function and energy are expressed as a power series in λ:

$$\Psi = \lim_{m \to \infty} \sum_{i=0}^{m} \lambda^i \Psi^{(i)} \tag{2.23}$$

$$E = \lim_{m \to \infty} \sum_{i=0}^{m} \lambda^i E^{(i)} \tag{2.24}$$

The MP method applies perturbations to HF by defining a *shifted* Fock operator $\hat{H}_0$ and *correlation potential* $\hat{V}$ as

$$\hat{H}_0 = \hat{F} + \langle \phi_0 | \left(\hat{H} - \hat{F} \right) | \phi_0 \rangle \tag{2.25}$$

$$\hat{V} = \hat{H} - \hat{H}_0 \tag{2.26}$$

where ϕ_0 is the ground state Slater determinant of the Fock operator.

Within this formulation, the zeroth-order energy is the expectation of $\hat{H}$, which gives the HF energy. The first order energy is

$$E_{MP1} = \langle \phi_0 | \hat{V} | \phi_0 \rangle = 0 \tag{2.27}$$

by Brillouin's Theorem of singly excited determinants. Thus, the first useful correction occurs at the second order of perturbation, which is known as MP2. Additional orders of perturbation are referred to as MPN. The MP2 method has been popular in quantum chemistry because it scales with N^5 number of basis functions and can be systematically improved with greater orders of perturbation.

Configuration interaction and coupled cluster theory

The solutions to the HF method give a single determinant wave function which only describes the ground state electronic configuration. Configuration interaction (CI) is a post-HF method which describes a linear combination of Slater determinants to more accurately represent a system's wave function. The additional Slater determinants represent excited electronic

configurations and can be singly excited (S), doubly excited (D), and so forth. This is represented as follows:

$$|\Psi\rangle = c_0 |\Psi_0\rangle + \sum_{ar} c_a^r |\Psi_a^r\rangle + \sum_{a<b,\ r<s} c_{ab}^{rs} |\Psi_{ab}^{rs}\rangle + \dots \tag{2.28}$$

where c is a coefficient for each determinant, and $a, b, \dots$ are indices for the orbitals from the electrons which are excited and $r, s, \dots$ are indices for the orbitals to which electrons are excited.

If all possible excitations are included in the CI equation, this is referred to as *full CI* (FCI). Extending FCI to an infinite basis set gives the exact solution to the Schrödinger equation.

Coupled cluster (CC) theory[90] is a similar approach to CI, but uses the so-called *exponential ansatz*

$$|\Psi\rangle = e^{\hat{T}} |\phi_0\rangle \tag{2.29}$$

where $\hat{T}$ is the cluster operator, defined by n-electron excitation operators $\hat{T}_n$:

$$\hat{T} = \hat{T}_1 + \hat{T}_2 + \hat{T}_3 + \dots \tag{2.30}$$

Within the exponential ansatz, $e^{\hat{T}}$ is usually truncated and expanded in a Taylor series. For example, truncation at the $\hat{T}_2$ excitation operator gives

$$\begin{aligned} |\Psi\rangle &= e^{\hat{T}_1 + \hat{T}_2} |\phi_0\rangle \\ &= (1 + \hat{T}_1 + \hat{T}_2 + \frac{1}{2!}\hat{T}_1^2 + \hat{T}_1\hat{T}_2 + \frac{1}{2!}\hat{T}_2^2 + \dots) |\phi_0\rangle \end{aligned} \tag{2.31}$$

Considering both CI and CC with single and double excitation (CISD and CCSD), the wave functions will include similar excitations, however inclusion of cross terms ($\hat{T}_1\hat{T}_2$) in CCSD implicitly includes higher excitation levels. This intrinsic benefit has driven CC to supersede CI as the method of choice for electron correlation calculations.

The inclusion of higher order excitations becomes decreasingly important with degree of excitation; however, the inclusion of triples is often found to be necessary for the accurate description of electron correlation (i.e. CCSDT). The computation of triples is prohibitively expensive in all but the simplest of systems, thus approximations based on perturbation theory are often used in substitution. The most commonly used perturbative triples method is CCSD(T), where the parenthesis indicate the use of

perturbative arguements. Note also that tradtionally, the use of CCSD(T) implies excitiation of only the valence electrons, unless otherwise stated.

CCSD(T) is commonly referred to as the *gold standard* in quantum chemistry and is often used to obtain benchmark quality results for thermochemistry and NCIs.[91] However, CCSD(T) scales with N^7 number of basis functions, and is thus significantly more computationally expensive than HF or MP2, restricting its application to small systems of molecules.

2.1.7 The complete basis set limit

Complete basis set extrapolation

In accordance with the variational principle, the energy obtained by a particular method will always be greater than or equal to the exact energy. The exact energy can only be achieved with an infinite basis set, a value known as the *complete basis set* (CBS) limit.[92] Since this is computationally infeasible, specific tricks have been developed to approximate the CBS limit. Specifically, molecular properties calculated using the HF and post-HF methods have been shown to asymptotically approach the CBS limit in a smooth manner when appropriate basis sets are used. Therefore, to obtain results estimating a molecular property at the CBS limit ($Y(\infty)$), properties can be fit to three-parameter[93,94] or two-parameter functions:[95,96]

$$Y(x) = Y(\infty) + Ae^{-x/B} \tag{2.32}$$

$$Y(x) = Y(\infty) + A/x^3 \tag{2.33}$$

where the molecular property as a function of basis set cardinal number $Y(x)$ is fit using parameters A and B. Typically calculations of this nature are performed using the correlation consistent basis sets (cc-pVNZ), however there is evidence that the polarisation consistent basis sets (pc-X) more rapidly approach the CBS limit for some molecular properties.[97] The true *gold standard* in quantum chemistry is referred to as CCSD(T)/CBS, which typically means CCSD(T) with complete basis set extrapolation with aug-cc-pVNZ basis sets, where N=D, T, Q, or 5. Although extrapolation is useful for approximating highly accurate results, there is an inherent amount of uncertainty associated with the final fitted results, which may be unclear from the nomenclature.

Explicit correlation methods

A new technique which is gaining popularity among post-HF methods is the inclusion of so called *explicit correlation.*[98,99] The introduction of additional functions dependent on inter-electronic distance coordinates allows for explicit correlation of electrons.[100] As a result, the dynamical correlation of electrons is treated more accurately with reduced basis sets, therefore accurate results can be achieved at a reduced computational cost. Basis set extrapolation can also be performed on explicitly correlated results: this is quickly become the standard approach.[101]

2.1.8 Composite quantum chemistry methods

In order to confidently calculate thermochemical and kinetic properties that are within a sub-kcal mol^{-1} range of experiment, multistep *ab initio* procedures which are referred to as *composite methods* have been developed.[102] These procedures work by including important energy terms which contribute to molecular properties. Some of the relevant energy terms include: core-valence, relativistic, spin-orbital, Born-Oppenheimer, and zero-point vibrational energy corrections. Each composite method makes use of a variety of quantum mechanical (QM) methods and uses of basis set extrapolation in order to best approximate energy terms which are relevant. In our work, we have made use of several composite methods including: the G4 and G4(MP2) methods,[103,104] CBS-QB3 and CBS-APNO methods,[105–107] and the W1BD method.[108]

2.1.9 Density-functional theory

Density-functional theory (DFT) is the most popular quantum chemical method applied to date. It relies on the two Hohenberg-Kohn theorems, the first of which states that there exists a unique electron density ρ that defines the properties of a many-electron system. The second theorem defines an energy functional of the electron density and demonstrates that the correct ground state electron density minimises the energy functional through the variational theorem.[109,110] These theorems alone do not provide the solutions to the Schrödinger equation.

It wasn't until the formulation of Kohn-Sham DFT[111] that the theory began gaining ground as a useful quantum theory. Kohn-Sham DFT scales formally with N^3 number of basis functions[89] which is better than HF by a factor of N. In addition, DFT is a complete theory like FCI; however, there is no straightforward way to determine the correct functionals of the

electron density. Nonetheless, the drive for the correct density-functional has been one of the main endeavours in quantum chemistry in the last two decades.

The framework behind conventional DFT is built into the description of the full energy functional E:

$$E[\rho] = T_{ni}[\rho] + V_{ne}[\rho] + V_{ee}[\rho] + \Delta T[\rho] + \Delta V_{ee}[\rho] \tag{2.34}$$

where T_{ni} is the kinetic energy of non-interacting electrons, V_{ne} is the potential of nuclear-electron interactions, and V_{ee} is the classical electron-electron repulsion. The last two terms are collectively referred to as the exchange-correlation (XC) functionals, where ΔT is the dynamical correlation term, and ΔV_{ee} is the non-classical correction to electron-electron repulsion. All the functionals, except the XC functionals have an exact form. It is therefore the XC functionals in which there in currently empiricism.

Ignoring the problem of choosing functionals, solving DFT is computationally very similar to the HF method. The electron density is formed from a linear combination of basis functions composed of GTOs, and the energy comes out from iteratively solving the eigenvalues of the Kohn-Sham pseudo-eigenvalue equation for orbitals χ:

$$\hat{h}_i^{KS}\chi_i = \varepsilon_i\chi_i \tag{2.35}$$

where a Kohn-Sham operator $\hat{h}^{KS}$ is defined as

$$\hat{h}_i^{KS} = -\frac{1}{2}\nabla_i^2 - \sum_k^{nuclei} \frac{Z_k}{|\mathbf{r}_i - \mathbf{R}_k|} + \int \frac{\rho(\mathbf{r\prime})}{|\mathbf{r}_i - \mathbf{r\prime}|} d\mathbf{r\prime} + V_{XC} \tag{2.36}$$

and

$$V_{XC} = \frac{\delta E_{XC}}{\delta \rho} \tag{2.37}$$

where V_{XC} is a functional derivative which describes the exchange-correlation energy.

Currently there are too many published XC functionals to list. Fortunately, there is a fairly standard system of nomenclature, such that density functionals are described as *exchange functional-correlation functional*. The most commonly used density functional is B3-LYP, which uses the 3-parameter exchange functional of Becke,[112] and the correlation functional of Lee, Yang, and Parr.[113] There are also standalone functionals which have

built in exchange and correlation functionals. A common example of these are the Minnesota family of functionals from the Truhlar group.[114,115]

There are several classes of density functionals including pure functionals, hybrid functionals, and range-separated functionals. Pure functionals are those that depend only on the density (ρ) of a system. Many DFT functionals incorporate a percentage of HF exact-exchange into their formulation. If a fixed percentage of exact-exchange is used, these are referred to as hybrid functionals. B3LYP is an example of a hybrid functional which has 20% HF exchange. Functionals which have a different amount of exact-exchange to describe long and short range behaviours are known as range-separated hybrid functionals. A popular example of a range-separated functional is known as CAM-B3LYP,[116] which is a long range corrected version of the B3LYP functional. While the incorporation of HF-exchange into DFT procedures can improve the accuracy of a method, it does come with an increased computational cost.

Challenges for density-functional theory methods

The allure of DFT is clear, given its relatively low computational cost and reasonable accuracy. However, there are several problems which common DFT methods experience that lead to erroneous results in many cases.[117] It is well established that traditional DFT methods completely fail at describing non-covalent interactions.[118] This shortcoming leads to poor descriptions of chemistry beyond equilibrium geometries, including transition states. Fortunately, there are several methods which can correct for this problem, commonly through the addition an energy correction term E_{disp} to the DFT energy E_{DFT}, as

$$E_{tot} = E_{DFT} + E_{disp} \tag{2.38}$$

The is most commonly done employing the empirical D3 pair-wise correction of Grimme,[119] paired with of the Becke-Johnson damping functions,[120] denoted as D3(BJ). This correction works by calculating the dispersion interactions between all pairs of atoms A and B separated by distance R_{AB}, with the following equation:

$$E_{disp} - \sum_{A>B} \frac{C_6^{AB}}{R_{AB}^6} f_6(R_{AB}) + s_8 \frac{C_8^{AB}}{R_{AB}^8} f_8(R_{AB}) \tag{2.39}$$

where C_6 and C_8 are dispersion coefficients , s_8 is an empirically determined scaling parameter, and f_n are the damping functions which limit the range

of dispersion correction, avoiding near singularities at small R_{AB}. Another approach to correcting for dispersion is to add parameters directly to the functional, as is the case in the Minnesota functionals.[114,114] These empirical corrections have the benefit of adding minimal computational time, but must be parametrised for each DFT method for which they are employed with.

Another striking issue with DFT is the unphysical ability of an electron to interact with itself, termed *self-interaction error*. This is most obvious in what is known as *delocalisation error*, which is a result of many-electrons interacting with themselves, or many-electron self-interaction error. In HF theory, self-interaction error is exactly cancelled, thus DFT methods which have a high portion of HF exchange in their formulation are able to account for this issue. The most obvious manifestation of delocalisation error is incorrect treatment of charge-transfer in intramolecular interactions.[121,122] Charge-transfer occurs when a fraction of an electron is transferred between molecular entities. Specifically, charge-transfer is mistreated at longer ranges, thus range-separated functionals are suggested for systems in which charge-transfer may occur.

2.2 Applying theory to chemical problems

2.2.1 Geometry optimisation

All QM methods depend parametrically on the geometry of a molecular system. While the wave functions can describe any arbitrary geometry, we are typically only interested in certain geometries of a molecule. These geometries of interest are normally stationary states along a the potential energy surface of a system, that is, points where the gradient of energy with respect to nuclear coordinates is zero. Therefore, we perform *geometry optimisation* calculations to determine these points.

As previously described, molecules have complex PESs. For a non-linear molecule, the nuclear PES has $3N$-6 dimensions, where N is the number of nuclei present.[123] In geometry optimisation, we seek the local minima (reactants, products, or intermediates) and local maxima (TS complexes). Consider only local minima for a moment. Often complex molecules have more than one possible conformation, and each conformation represents a different local minimum along the PES. It is therefore important to ensure the correct conformation, typically the lowest energy structure (global minimum), is used when approaching chemical problems.

Some additional caution must be taken in optimising molecular structures. Normal algorithms which optimise structures stop when the gradient

of energy is sufficiently close to zero; however, often PES can be flat or very shallow in regions and non-optimised structures can be obtained. To overcome this, geometries are always subject to molecular vibration analysis.

2.2.2 Molecular vibrations

The computation of molecular vibrations can be performed simply given a set of molecular coordinates.[124] Assuming a non-linear molecule, we start with $3N$-6 internal coordinates which are non-coupled (orthogonal). We then apply the *harmonic approximation*, in which we assume each normal mode follows Hooke's Law

$$F = kx \tag{2.40}$$

where F is the force, k is the force constant, and x is the displacement along one normal mode's coordinates. This approximation assumes the PES along the normal mode is parabolic, which in general is not true. Deviations from this approximation are known as *anharmonicity*. In practise however, at normal temperatures ($\sim$ 298K) the harmonic approximation is sufficient to describe molecular vibrations as displacements are assumed to be small.

Typically to obtain molecular frequencies, one computes the mass-weighted Hessian matrix elements F_{ij}

$$F_{ij} = \frac{1}{\sqrt{m_i m_j}} \frac{\partial^2 U}{\partial x_i \partial x_j} \tag{2.41}$$

where the partial derivatives of internal coordinates x_i of the potential energy U are taken for $3N$ atoms with mass m. One then seeks to diagonalise this $3N \times 3N$ matrix to obtain eigenvalues λ_i, which describe the force constant of each normal mode. The harmonic frequencies ν_i are then obtained by

$$\nu_i = \frac{\sqrt{\lambda_i}}{2\pi} \tag{2.42}$$

and the lowest 6 vibrations are then discarded to account for $3N$-6 normal modes.

From these frequencies, the *zero-point vibrational energy* (ZPE, E_{ZPE}) is calculated:

$$E_{ZPE} = \sum_{i=1}^{3N-6} \frac{h\nu_i}{2} \tag{2.43}$$

The ZPE is an important quantum correction to the classical potential, giving the electronic potential energy

$$U = E_{elec} + E_{ZPE} \tag{2.44}$$

where E_{elec} is the QM electronic energy.

If a normal mode describes a non-minimum along the PES, the energy gradient will be negative (imaginary) instead of positive. Only energy maxima or saddle-points (TS structures) should have a single imaginary mode. Therefore, if a non-TS molecular structure calculation yields one or more imaginary modes, the geometry optimisation has yielded a structure which is not at minimum on the PES. In this situation additional steps must be taken to find a corrected structure.

2.2.3 Thermochemistry

Up until this point we have been viewing molecules from a microscopic perspective; however, this is not useful for describing properties of bulk systems. Fortunately, fundamental statistical thermodynamics can be used to approximately describe a system in bulk.[125,126] We approximate our system as an ensemble of non-interacting particles: the ideal gas. Within statistical thermodynamics, the fundamental starting point is the partition function Q,[127] from which all thermodynamic properties can be calculated. For our ensemble, the molecular partition function is

$$Q = \sum_{J} e^{\varepsilon_j / k_B T} \tag{2.45}$$

where a Boltzmann distribution of j energy states ε is taken at temperature T, and k_B is the Boltzmann constant. All calculations herein are defined under conditions of temperature $T = 298.15$ K and pressure $P = 1$ atm.

Normally, the molecular partition function is decomposed into contributions from translational, vibrational, rotational, and electronic motion:

$$Q = q_{trans} q_{vib} q_{rot} q_{elec} \tag{2.46}$$

The equation describing the translational partition function q_{trans} is

$$q_{trans} = \left(\frac{2\pi m k_B T}{h^2} \right)^{3/2} \frac{k_B T}{P} \tag{2.47}$$

where m is the mass of the molecule, h is Planck's constants.

The vibrational partition function q_{vib} depends on the contributions of each of K vibrational modes. Only the $3N-6$ (or $3N-5$ for linear molecules) real vibrational modes of a molecule are considered, and imaginary frequencies are ignored. Therefore, for molecules which posses an imaginary frequency (excluding TS-complexes) this thermodynamic analysis is invalid. Each vibrational mode has a characteristic vibrational electronic temperature, $\Theta_{\nu,K} = h\nu/k_B$, and the partition function is

$$q_{vib} = \prod_K \frac{e^{-\Theta_{\nu,K}/2T}}{1 - e^{-\Theta_{\nu,K}/T}} \tag{2.48}$$

The rotational partition function depends on the geometry of a system. For a single molecule q_{rot}=1. For a linear molecule, the rotational partition function is

$$q_{rot} = \frac{1}{\sigma_r}\left(\frac{T}{\Theta_r}\right) \tag{2.49}$$

where σ_r is the symmetry number for rotation which depends on the molecular symmetry, and $\Theta_r = h^2/8\pi^2 I k_B$. I is the moment of inertia. Finally, for a non-linear polyatomic molecule, the rotational partition function is

$$q_{rot} = \frac{\sqrt{\pi}}{\sigma_r}\left(\frac{T^{3/2}}{\sqrt{\Theta_{r,x}\Theta_{r,y}\Theta_{r,z}}}\right) \tag{2.50}$$

where $\Theta_{r,x}, \Theta_{r,y}$, and $\Theta_{r,z}$ describe contributions of the moment of inertia in each of the x, y, and z-planes.

Finally, we make an important assumption that electronic contributions are assumed to exist in only the ground state, as excited states are generally safely assumed to be much larger than $k_B T$ in energy. The full electronic partition function is

$$q_{elec} = \sum_{i=0} \omega_i e^{-\epsilon_i/k_B T} \tag{2.51}$$

where ω is the degeneracy of an energy level with energy ϵ. Applying our assumption, and by setting the ground state energy $\epsilon_0 = 0$, our problem simplifies dramatically, such that $q_{elec} = \omega_0$, which is simply the spin multiplicity of the molecule.

We now have all the information needed to calculate the thermodynamic quantities we are interested in. In chemistry we are concerned with the Gibbs free energy G, which is defined by the entropy S and enthalpy H as

$$G = H - TS \tag{2.52}$$

From each of the partition functions, the entropy of a system with N moles, $S_{tot} = S_{trans} + S_{vib} + S_{rot} + S_{elec}$, is calculated using the relation

$$S = Nk_B + Nk_B \ln\left(\frac{Q}{N}\right) + Nk_BT\left(\frac{\partial \ln Q}{\partial T}\right)_V \tag{2.53}$$

Similarly, the internal energy of a system, $E_{int,tot} = E_{int,trans} + E_{int,vib} + E_{int,rot} + E_{int,elec}$, is given by the relation

$$E_{int} = Nk_BT^2\left(\frac{\partial \ln Q}{\partial T}\right)_V \tag{2.54}$$

Finally, the enthalpy is obtained from

$$H_{tot} = E_{int,tot} + k_BT \tag{2.55}$$

Using very simple statistical thermodynamic arguments, the properties of a bulk system are easily computed. It is important to emphasise that these results are for particles in the gas phase, thus additional steps must be taken if one desires to compare results to experiments performed in solvent.

2.2.4 Modelling solvent

It is in principle possible to include solvent models explicitly in QM calculations: this is in practise, extremely cost prohibitive. In order to approximate the important contributions of solvation, so-called *implicit continuum solvent models* are generally employed.[89,128] Mathematically, one describes this as

$$\hat{H}^{tot}(\mathbf{r}_m) = \hat{H}^{mol}(\mathbf{r}_m) + \hat{V}^{mol+sol}(\mathbf{r}_m) \tag{2.56}$$

where a perturbation $\hat{V}^{mol+sol}$ dependent only on the coordinates of the solute ($\mathbf{r}_m$; thus implicit) is applied to the Hamiltonian of the solute. The perturbation term is composed of interaction operators which contribute to the net free energy:

$$G_{solv} = G_{cavity} + G_{electrostatic} + G_{dispersion} + G_{repulsion} + G_{solv\ kinetic} \tag{2.57}$$

where the total solvation free energy G_{solv} contains terms from: the formation of a solvation cavity G_{cavity}, the electrostatic interactions between

solvent and solute $G_{electrostatic}$, the dispersion interactions between solvent and solute $G_{dispersion}$, the QM exchange repulsion between solvent and solute $G_{repulsion}$, and the movement of solvent molecules $G_{solv\ kinetic}$.

The most widely used model for solvation comes from the Truhlar group, and is known as SMD.[129] The main parameter in implicit solvent models is the solvent dielectric constant (ε) with contributions from surface tension and the solvent-solute interface. SMD also includes terms which depend on the electron density of the solute. While many other implicit solvent models require the use of the same QM method as they were parametrised,[130] SMD is a *universal* model which was parametrised using several QM methods. Therefore, it does not require the use of a specific QM method and can be applied broadly in both single point energy and geometry optimisation calculations.

2.2.5 Rate constants and transition state theory

In the discussion of chemical kinetics, the rate (r) of a bimolecular reaction

$$a\,\mathrm{A} + b\,\mathrm{B} \rightleftharpoons c\,\mathrm{C} + d\,\mathrm{D} \tag{2.58}$$

is determined by the *rate law*, which can generally be described as

$$r = \frac{d\mathrm{C}}{dt} = \frac{d\mathrm{D}}{dt} = k[A]^a[B]^b \tag{2.59}$$

where k is the rate constant, t is time, A, B, C, and D are chemical species with stoichiometric coefficients a, b, c, and d, and k is the rate constant. Computational chemistry is in general, not useful for determining rate laws: this must be done experimentally. Where computational studies can be useful, is in determining reaction mechanisms, and how the reaction barrier height can be altered. In doing so, we focus entirely on k.

Most chemists are intimately familiar with the phenomenological *Arrhenius equation*

$$k_{Arr} = Ae^{-E_a/RT} \tag{2.60}$$

where A is a constant, R is the gas constant, and E_a is the *activation energy*, which is an experimental measure of the reaction barrier height. This equation dates back to the 1880s, when Arrhenius noticed that the reactions depended more heavily on temperature than was intuitive, and thus introduced the A constant, known often as the Arrhenius pre-factor.[131]

The Arrhenius pre-factor is an empirical measure of how factors other than kinetic energy affect the rate constant. From the perspective of theory, Equation 2.60 has little meaning as the parameters are empirical. Thus, to study rate constants theoretically we must turn to *transition state theory*.

Transition state theory

The study of transition state theory (TST) originates in the 1930s, and was developed primarily by Eyring.[131,132] In TST we focus on the TS complex, which is defined as a transient species which exists at the top of the energy barrier of a reaction. If we consider the same reaction in Equation 2.58, and set all the coefficients to 1, then TST states the reaction proceeds in two steps, the first of which includes a quasi-equilibrium between the reactants and TS complex

$$\mathrm{A} + \mathrm{B} \rightleftharpoons \mathrm{AB}^{\ddagger} \longrightarrow \mathrm{C} + \mathrm{D} \tag{2.61}$$

with an equilibrium constant ($K_c^{\ddagger}$) expression

$$K_c^{\ddagger} = \frac{[\mathrm{AB}^{\ddagger}]/c^0}{[\mathrm{A}]/c^0[\mathrm{B}]/c^0} \tag{2.62}$$

where c^0 is the standard-state concentration (normally taken to be 1 M).

In TST, we define the TS complex to exist throughout a small region of width δ above the reaction barrier (Figure 2.1). From the second step of the reaction in Equation 2.61, we can define a reaction rate dependent on the concentration $[\mathrm{AB}^{\ddagger}]$ and v_c, a factor which defines the frequency with which the complexes proceed over the barrier:

$$r = v_c[\mathrm{AB}^{\ddagger}] \tag{2.63}$$

From Equations 2.58 and 2.61, we now have two equivalent expressions for the reaction rate, which allows us to derive the following

$$r = k[\mathrm{A}][\mathrm{B}] = v_c[\mathrm{AB}^{\ddagger}] \tag{2.64}$$

and solving Equation 2.62 for $[\mathrm{AB}^{\ddagger}]$ results in

$$r = v_c \frac{[\mathrm{A}][\mathrm{B}]K_c^{\ddagger}}{c^0} \tag{2.65}$$

or

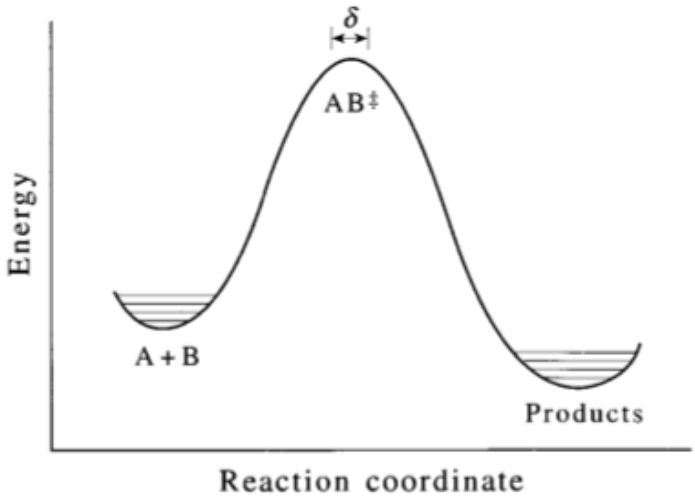

Figure 2.1: A reaction coordinate diagram for the reaction of Equation 2.61. The TS complex is defined to exist in the small region δ above the reaction barrier. Figure taken from Reference 131.

$$k = \frac{v_c K_c^{\ddagger}}{c^0} \tag{2.66}$$

We must now invoke the statistical thermodynamics to make sense of Equation 2.66. We can rewrite the equilibrium expression $K_c^{\ddagger}$ in terms of partition functions of each molecular species:

$$K_c^{\ddagger} = \frac{[\mathrm{AB}^{\ddagger}]/c^0}{[\mathrm{A}]/c^0[\mathrm{B}]/c^0} = \frac{(q^{\ddagger}/V)c^0}{(q_A/V)(q_b/V)} \tag{2.67}$$

where q_A, q_B, and $q^{\ddagger}$ are the partition functions of A, B, and $\mathrm{AB}^{\ddagger}$, respectively.

Since we have defined the reaction to be occurring with one degree of freedom, the translational partition function q_{trans} can be defined as

$$q_{trans} = \frac{\sqrt{2\pi m^{\ddagger} k_B T}}{h}\delta \tag{2.68}$$

where $m^{\ddagger}$ is the mass of the TS complex. The partion function of the TS complex can be written as the product $q^{\ddagger} = q_{trans}q_{int}^{\ddagger}$, where the second term accounts for all remaining degrees of freedom of the TS complex. We can use this and rewrite Equations 2.67 and 2.66 as

$$K_c^{\ddagger} = \frac{\sqrt{2\pi m^{\ddagger} k_B T}}{h} \delta \frac{(q_{int}^{\ddagger}/V)c^0}{(q_A/V)(q_b/V)} \tag{2.69}$$

and

$$k = v_c \frac{\sqrt{2\pi m^{\ddagger} k_B T}}{hc^0} \delta \frac{(q_{int}^{\ddagger}/V)c^0}{(q_A/V)(q_b/V)} \tag{2.70}$$

We are now left with the two terms v_c and δ which are ill-defined. However, the product of these two terms is the average speed at which the TS complex crosses the barrier, $\langle u_{TS} \rangle = v_c \delta$. A Maxwell-Boltzmann distribution is used to calculate the value of $\langle u_{TS} \rangle$:

$$\langle u_{TS} \rangle = \left(\frac{m^{\ddagger}}{2\pi k_B T} \right)^{1/2} \int_0^{\infty} u e^{-m^{\ddagger} u^2 / 2k_B T} du = \left(\frac{m^{\ddagger}}{2\pi k_B T m^{\ddagger}} \right)^{1/2} \tag{2.71}$$

Substituting Equation 2.71 into Equation 2.70 for $v_c \delta$ yields

$$k = \frac{\sqrt{k_B T}}{hc^0} \frac{(q_{int}^{\ddagger}/V)c^0}{(q_A/V)(q_b/V)} = \frac{k_B T}{hc^0} K_c^{\ddagger} \tag{2.72}$$

Now, define the standard Gibbs free energy of activation ($\Delta^{\ddagger} G^0$) to be the change in Gibbs free energy in going from reactants to TS. The thermodynamical expression is

$$\Delta^{\ddagger} G^0 = -RT \ln K_c^{\ddagger} \tag{2.73}$$

which can be substituted into Equation 2.72

$$k = \frac{k_B T}{hc^0} e^{-\Delta^{\ddagger} G^0 / RT} \tag{2.74}$$

The standard Gibbs free energy of activation can be expressed in terms of enthalpy and entropy as

$$\Delta^{\ddagger} G^0 = \Delta^{\ddagger} H^0 - T \Delta^{\ddagger} S^0 \tag{2.75}$$

which, upon substitution gives the equation

$$k = \frac{k_B T}{hc^0} e^{-\Delta^{\ddagger} S^0 / R} e^{-\Delta^{\ddagger} H^0 / RT} \tag{2.76}$$

At this point, we can draw a direct comparison to the Arrhenius equation (Equation 2.60) by expressing E_a in terms of $\Delta^{\ddagger} H^0$ and A in terms of $\Delta^{\ddagger} S^0$.

We must differentiate the natural logarithm of Equation 2.72, as well as Equation 2.60 (assuming that A is independent of temperature):

$$\frac{d\ln k}{dT} = \frac{1}{T} + \frac{d\ln K_c^{\ddagger}}{dT} \tag{2.77}$$

$$\frac{d\ln k_{Arr}}{dT} = \frac{E_a}{RT^2} \tag{2.78}$$

Next, we use the fact that $d\ln K_c/dT = \Delta U^0/RT^2$ for an ideal gas, then Equation 2.77 becomes

$$\frac{d\ln k}{dT} = \frac{1}{T} + \frac{\Delta^{\ddagger}U^0}{RT^2} \tag{2.79}$$

Additionally, $\Delta^{\ddagger}H^0 = \Delta^{\ddagger}U^0 + RT\Delta^{\ddagger}n$ ($\Delta^{\ddagger}n = 1$), as so Equation 2.79 can be rewritten as

$$\frac{d\ln k}{dT} = \frac{\Delta^{\ddagger}H^0 + 2RT}{RT^2} \tag{2.80}$$

Therefore, by comparison of Equation 2.80 and 2.78, we get

$$E_a = \Delta^{\ddagger}H^0 + 2RT \tag{2.81}$$

which then converts Equation 2.76 into the form

$$k = \frac{e^2 k_B T}{hc^0} e^{\Delta^{\ddagger}S^0/R} e^{-E_a/RT} \tag{2.82}$$

Therefore, a statistical thermodynamical picture of the Arrhenius equation arises from TST, and the Arrhenius pre-factor A can be expressed as

$$A = \frac{e^2 k_B T}{hc^0} e^{\Delta^{\ddagger}S^0/R} \tag{2.83}$$

In practise, we use the form of Equation 2.74 to compute the rate constant of a reaction, which we shall denote as k_{TST}. The conventional TST makes an assumption that the reaction coordinate is static along the lowest energy pathway. This can be corrected by the use of *variational transition state theory*.[133] We shall not consider variational TST in this work, as with careful application, conventional TST does a remarkably good job at accounting for the magnitude and temperature dependence of a wide range of reactions.[132] Additionally, if one makes corrections for *QM tunnelling*, conventional TST can easily give a more complete description of the rate constant.

Quantum mechanical tunnelling

Atoms are quantum mechanical particles, and are thus subject to the strange probabilistic behaviours observed at the microscopic level. QM tunnelling refers to the ability of particles to penetrate the reaction barrier, rather than surmounting it classically (Figure 2.2). While all reactions are subject to QM tunnelling, we will show that due to the low mass of the hydrogen atom, QM tunnelling can play a significant role in HAT reactions.

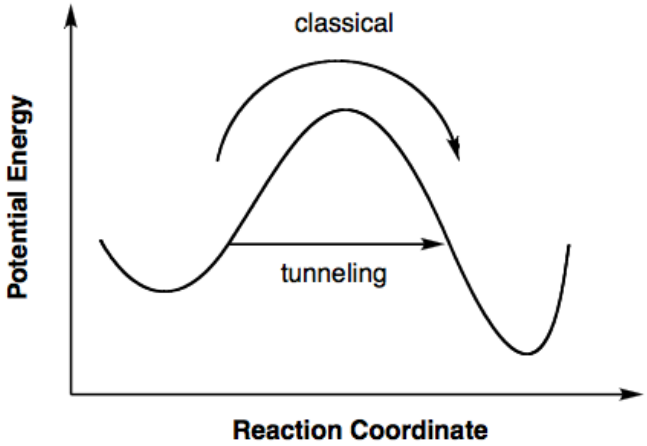

Figure 2.2: Quantum mechanical tunnelling occurs when a particle penetrates a reaction barrier, rather than surmounting it. (Place holder figure)

In order to determine the effects of scattering, one must find transmission coefficients (κ) by solving the Schrödinger equation. This is done by approximating the reaction barrier with an analytical potential, thus simplifying the problem mathematically. The earliest model potentials were introduced by Bell, who used a parabolic function to approximate the reaction barrier.[134] To obtain κ, and thus the observed rate constant (k_{obs}), the following equations were used:

$$k_{obs} = \kappa A e^{-E_a/RT} \tag{2.84}$$

$$\kappa = \frac{e^{\alpha}}{\beta - \alpha}\left(\beta e^{-\alpha} - \alpha e^{-\beta}\right) \tag{2.85}$$

$$\alpha = E_a/RT \tag{2.86}$$

$$\beta = \frac{2a\pi^2(2mE_a)^{1/2}}{h} \tag{2.87}$$

where the Arrhenius equation was used to estimate the rate constant, m is the mass of the tunnelling particle, and $2a$ is the width of the barrier. Since the equation is dependent on the mass of the particle, tunnelling occurs more often when lighter particles are involved. As a consequence, tunnelling is more common in HAT reactions than other atom transfer reactions. Also, the height and width of the barrier are important factors in determining the contributions to tunnelling: reactions with small barriers have low tunnelling contributions; narrow barriers result in higher tunnelling contributions.

The Bell model is a poor representation of an actual reaction barrier. One which is a much better approximation is the *Eckart potential*.[135] The form of this potential is

$$V = -\frac{Ay}{1-y} - \frac{By}{1-y^2} \tag{2.88}$$

$$y = -e^{2\pi x/L} \tag{2.89}$$

where x is the variable along the reaction coordinate and L is called the characteristic length. If $A = 0$ the potential becomes a symmetric function, further simplifying the problem; however, most reactions do not have a symmetric potential. A, B and L are related to the change in barrier height in the forward and reverse direction, $\Delta V1$ and ΔV_2, respectively:

$$A = \Delta V_1 - \Delta V_2 \tag{2.90}$$

$$B = ((\Delta V_1)^{1/2} + (\Delta V_2)^{1/2})^2 \tag{2.91}$$

$$\frac{L}{2\pi} = (-\frac{2}{F^*})^{1/2}[\frac{1}{(\Delta V_1)^{1/2}} + \frac{1}{(\Delta V_2)^{1/2}}]^{-1} \tag{2.92}$$

where $F^* = d^2V/dx^2$ evaluated at the maximum of the potential. In this formulation, V is a placeholder energy. Note that if a reaction is endoergic, tunnelling does not occur. Alteratively, one says tunnelling only occurs in exoergic or energy-neutral reactions.

The solutions to the Schrödinger equation for the Eckart potential are analytical, thus that transmission coefficient κ can easily be computed using standard numerical techniques. These tunnelling corrections will be applied, where applicable as

$$k_{calc} = \kappa k_{TST} = \kappa \frac{k_B T}{hc^0} e^{-\Delta^\ddagger G^0} \tag{2.93}$$

Chapter 3

Methods

In this chapter, we shall briefly outline the procedures and computational methods used to obtain the results in this thesis. The methods have been broken down in a per chapter manner. All quantum mechanical calculations were performed using either the Gaussian 09[136] or TURBOMOLE programs.[88] Molecular structures were built in the GaussView program.[137] Optimised structures were verified local minima by vibrational analysis and visualised using the Chemcraft program.[138] Transition state structures were all verified saddle points by visualisation of a single imaginary frequency connecting reactants to products. As a brief note on notation, computational methods used are described using the following notation: *method*/*basis*, for example, calculations performed using the B3LYP density functional with 6-31+G* basis sets is denoted as B3LYP/6-31+G*. Commonly, single-point energy calculations with a higher level of theory (*HL method* and *HL basis*) are performed on structures optimised with a lower level of theory (*LL method* and *LL basis*), this is denoted as *HL method*/*HL basis*//*LL method*/*LL basis*. Thermochemical corrections are also taken from the lower level of theory.

3.1 Chapter 4

In this chapter, we seek to calculate pre-reaction complex binding energies for bulky phenolic or peroxylic substrates which participate in nearly thermoneutral reactions. Conformational analysis to locate the global minimum substrate geometry was performed using the BLYP-D3(BJ) method[113,119,120,139] utilising the minimal MINIs basis sets[140] and our groups own *basis set incompletion potentials* (BSIPs).(citation needed) Geometries were manipulated by manual rotation of the necessary dihedral bond angles, followed by geometry optimisation and vibrational analysis.

The lowest energy substrates were combined to generate the appropriate pre-reaction complexes. These pre-reaction complexes were subject to conformational analysis using the same BLYP-D3(BJ)-BSIP/MINIs method. Geometries were initially manipulated by hand. It became apparent that

manual manipulation resulted in an unsatisfactory exploration of the conformational space. To overcome this, all the necessary dihedral angles were scanned systematically using a combination of scripts.[141] All manipulated geometries were subject to optimisation. For each complex, the top 5-10 complex geometries were subject to further optimisation using a higher level of theory (BLYP-D3(BJ)/pc-1) to obtain the final minimum energy pre-reaction complex structures.(currently some non-minimum structures)

To obtain accurate pre-reaction complex binding energies, the substrates and complexes were subject to single-point energy calculations using the LC-ωPBE long-range corrected density functional[142,143] with D3(BJ) dispersion corrections and pc-2 basis sets with truncated f-type functions (pc-2-spd).[144] This method was selected on the recommendation of work by Johnson et al.[144], which demonstrated that this was an efficient method for calculation NCIs with a reasonable degree of accuracy.

3.2 Chapter 5

In this chapter, we probe the applicability of the Bell-Evans-Polanyi principle in two broad classes of C-H bond hydrogen atom transfer reactions with CumO$^{\bullet}$. In order to do this, we seek to calculate BDEs which are *chemically accurate*, that is, within 1 kcal mol^{-1} of the "true value." To achieve this, the highly accurate W1BD[108] quantum mechanical composite method was employed.

Unfortunately, some of the substrates of interest are too large to be treated with the W1BD method, thus we sought a less computationally expensive method which most gave results of comparable precision. There is currenly no literature which benchmarks computational procedures for bond dissociation enthalpies. As a consequence, we explored a variety of other quantum mechanical composite methods, including: the G4 and G4(MP2) methods,[103,104] and the CBS-QB3, ROCBS-QB3, and CBS-APNO methods.[105–107]

(Is the LDBS approach relevant if we didn't use it for analysus in the end?) Additionally, we developed a method which we call the *locally dense basis set approach* (LDBS), which makes use of the ROCCSD(T) method with a basis set partitioning scheme. The partitioning scheme is as follows: groups which are close the the bond being broken are treated with large basis sets (pc-3), while groups which are further away have incrementally smaller basis sets. Specifically, we use a 3/2/1 partitioning, such that the carbons centred group where bond dissociation occurs, as well as the groups

immediately adjacent, are treated with the high-level pc-3 basis sets. The next groups over are treated with the medium-level pc-2 basis sets. Any groups beyond this are treated with the low-level pc-1 basis sets. This is illustrated in Figure 3.1.

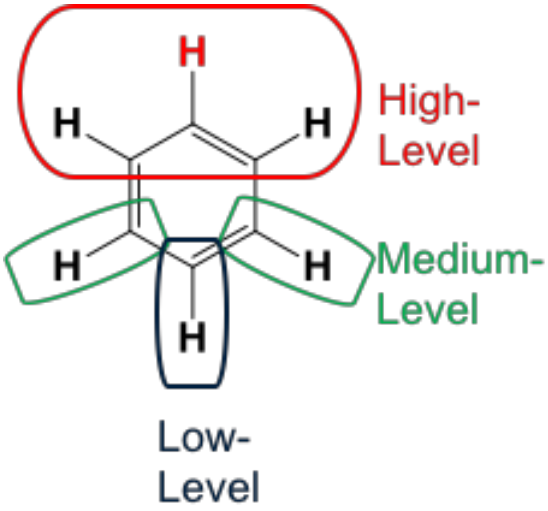

Figure 3.1: Example locally dense basis set partitioning on benzene used in the LDBS approach. The red hydrogen is that which is abstracted. High-level=pc-3, medium-level = pc-2, low-level = pc-1.

The performance of all methods was compared to both the W1BD calculated BDEs, as well as with experimentally available values, compiled from the *Handbook of Bond Dissociation Energies.*[145] Experimental values are obtained using a wide variety of techniques, some of which may not be entirely reliable. For example, thermochemical cycles[146] are often used to measure BDEs, however, this method has been shown to be unreliable if the reaction used occurs by PCET rather than direct HAT.[24] For this reason, a secondary goal of this work is to identify any experimental BDEs which may be in question.

To further probe the priniciples underlying the HAT reactions involved, TS structures for the HAT reaction with CumO$^{\bullet}$have been obtained for a large number substrates. TS structures were obtained using the B3LYP-D3(BJ)/6-31+G* method. Where possible, TS structures were obtained for both a cisoid and transoid conformation of the substrate/CumO$^{\bullet}$couple. Substrates and TS complexes were subject to single-point energy calculations at the LC-ωPBE-D3(BJ)/6-311+G(2d,2p) level of theory to obtain

more reliable reaction barrier heights.

3.3 Chapter 6

In this chapter, we seek to understand the effects of non-redox active metal cations of the hydrogen atom transfer reactions involving various organic substrates with oxygen centred radicals. As shall be discussed in Chapter 6, there is little literature which addresses the issue of interactions between organic substrates and alkali and alkaline earth metals. To address this, a benchmark study has been performed.

3.3.1 Benchmark study of non-redox active metal cations with organic substrates

The benchmark set shall be discussed in detail in Chapter 6. In order to avoid erroneous charge transfer from the possible charge transfer involved in cation-substrate interactions, conformational analysis was performed by manual geometry manipulation using the LC-ωPBE-D3(BJ)/6-31+G** method.[147] The most stable conformations of metal-substrate complexes was subjected to higher-level optimisation at the LC-ωPBE-D3(BJ)/6-311+G(3df,3pd) level of theory.

Initially, binding energy for the metal-substrate complexes was calculated using the full electron CCSD(T)/CBS approach, utilising two-point basis set extrapolation with aug-pc-3 and aug-pc-4 basis sets. These results showed systematic problems in the convergence of basis sets to the complete basis set limit for the alkali and alkaline earth metals. To address this, the binding energies were re-calculated using the full electron CCSD(T)-F12* explicitly correlated approach[148] with Def2-QZVPPD basis sets.

A variety of DFT methods and basis sets were benchmarked against the CCSD(T)-F12*/Def2-QZVPPD results (see Appendix (BLANK) for full details). Single point energy calculations were performed on LC-ωPBE-D3(BJ)/6-311+G(3df,3pd) structures. The validity of these structures was tested by re-optimisation with the three best performing DFT methods relative to the benchmark data (M05-2X, BMK-D3(BJ), and ωB97X-D with large basis sets). The average root mean square deviation in geometry was found to be onle 0.007-0.008 Å for all three methods, thus validating the structures. We elected to move forward using the M05-2X functional on the basis of the results obtained from the benchmark study of metal cation-substrate interactions, and the well described ability of M05-2X to accurately describe HAT reactions involving oxygen centred radical.[149]

3.3.2 Effects of metal cations on hydrogen atom transfer barrier heights

Chapter 4

The Relationship Between Arrhenius Pre-factors with Non-Covalent Binding

Chapter 5

Interrogation of the Bell-Evans-Polanyi Principle: Investigation of the Bond Dissociation Enthalpies correlated with Hydrogen Atom Transfer Rate Constants

Experimental BDEs from Bordwell[146] cycle are possible unreliable in the case where PCET occurs[24]

$$\mathrm{H\text{–}A} \rightleftharpoons \mathrm{H^+} + \mathrm{A^-} \qquad pK_{HA} \qquad (1)$$

$$\mathrm{A^-} \rightleftharpoons \mathrm{e^-} + \mathrm{A^\bullet} \qquad E_{ox}(\mathrm{A^-}) \qquad (2)$$

Increase/Reduce Image Size (3)

$$\mathrm{H\text{–}A} \rightleftharpoons \mathrm{H^\bullet} + \mathrm{A^\bullet} \qquad \mathrm{BDE} \qquad (4)$$

$$\Delta\mathrm{BDE} = 1.37\Delta pK_{HA} + 23.06\Delta E_{ox}(\mathrm{A^-}) \qquad (5)$$

Chapter 6

Do non-redox active metal cations have the potentials to behave as chemo-protective agents? The Effects on Metal Cations on HAT Reaction Barrier Heights

6.1 Benchmarking Density Functional Theory for the Binding of Alkali and Alkaline Earth Metals

In order to study the central hypothesis propsed in this work, we must carefully select a computational method. In particular, we wish to use density-functional theory (DFT), which is known to be prone to various problems such as self-interaction error,[150] delocalization error,[122] and the inability to treat non-covalent interactions.[118,151] The latter of these can be corrected by the selection of a method capable correcting the non-covalent corrections such as a pair-wise dispersion model (\-citeD3), or atom centered potentials developed by our group (\-citeDCPS). Other errors can be ignored through the careful selection of a DFT method.

We are interested in selecting a method which can accurately treat the interactions between alkali and alkaline earth metal cations, and organic substrates and radicals. To this end, there exists little literature, with one notable paper[152] which examines the binding of calcium cations to organic substrates. In this paper, Suárez et al.[152] provide accurate energetic, electronic, and structural results for the binding of calcium to organic neutral and charged species, as well as assess the performance of four different

DFT methods. They also analyze the nature of ligand-metal bonding interactions using a symmetry-adapted perturbation theory approach (SAPT) (EXPAND ON THIS)

Due to our interest in alkali and alkaline earth metal cations in FHT, we determined it necessary to prepare benchmark quality data for binding to organic substrates and radicals.

(Calcium prefers to bind to O, with binding to S or N is rare[153]) In N,N-dimethylacetamide for example, calcium binds preferentially to the lone pairs of the carbonyl oxygen over the nitrogen lone pair. This is shown in Scheme 6.1.

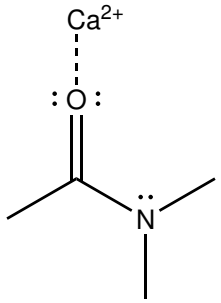

Scheme 6.1: Binding of the calcium cation (Ca^{2+}) to the oxygen lone pairs of N,N-dimethylacetamide.

6.1.1 Methods

Conformers were generated using Hyperchem with the AM1 semi-empirical molecular orbital (MO) method (\-citehyperchem) followed by optimization calulations of 5-10 lowest energy structures using at the ((currently unpublished)) BLYP-D3/pc1 level of theory, including our own groups basis set incomplete potential (BSIPs).((CITATIONS))

On the basis of the work by Otero-de-la-Roza et al.[122], which showed that in systems which are halogen bonded, erroneous charge transfer can be significant, and given the charge on the metal cations, the LC-ωPBE density functional with D3 dispersion correction and moderate 6-31+G(2d,2p) ((CITATIONS for DFT and D3)) basis sets were applied to determine the most strongly bound complexes of substrates and metal cations. Global minima monomers and complexes were optimized with the LC-ωPBE-D3 method near the basis set limit (6-311+G(3df,3pd). Highly correlated wavefunction results were obtained at the CCSD(T) level of theory with extrapolation to

the complete basis set limit.(CITATION) Calculations were performed using the Gaussian 09 package,[136] and wavefunction calculations were performed using the TURBOMOLE[88] package.

6.1.2 Benchmark systems

The purpose of this work is to provide high-level binding energies for organic substrates which are of interest directly for this project, but also which may be useful for future work. The substrates proposed were to be relevant to simple biological models such as dipeptide like molecules and the hydroxyl and hydroperoxyl radical. We also wanted to incorporate substrates with are important to the physical organic experiments that are performed to probe these systems, thus solvents such as acetonitrile and dimethylsulfoxide and the benzyloxyl and cumyloxyl radicals were also included. This set is shown in Scheme 6.2(FIND CDX).

Benchmark quality binding energies are generally calculated using the "gold standard" approach, CCSD(T)/CBS, where correlation consistent basis sets((CITATION)) (cc-pVXZ, X=T,Q,5) developed by Dunning and coworkers are used for complete basis set extrapolation. These basis sets have limited availability for the metals of interest. Specifically, basis sets for K are note available, and only non-augmented basis sets for Li, Na, Mg, and Ca. It is necessary to include core correlation of the n-1 shell in alkali and alkaline earth metals, thus it is advantageous to use core valence basis sets such as cc-pCVXZ. These basis sets are even more limitted, thus we opted for the augmented version of the polarization consistent basis sets of Jensen and co-workers (aug-pc-N, N=2,3,4). (CITATIONS FOR GOLD STANDARD AND BASIS SETS, NEED THEORY SECTION ON DIFFERENT BASIS SETS)

While performing CCSD(T)/CBS calculations, we notices that the metal cations (and neutral metal atoms), did not converge smoothly to the complete basis set limit. Given this, and the limitted computational resources, we decided to re-evaluate the size scope of the benchmark set being used. In order to facilitate future DFT work and probe the issue of basis set convergence of alkali and alkaline earth metals, a benchmark set of small substrates was proposed. This new set is shown in Scheme 6.3. The new, small benchmark set was selected to include important functional groups and radicals for biological systems and the most common solvent used in physical organic experiments, acetonitrile.

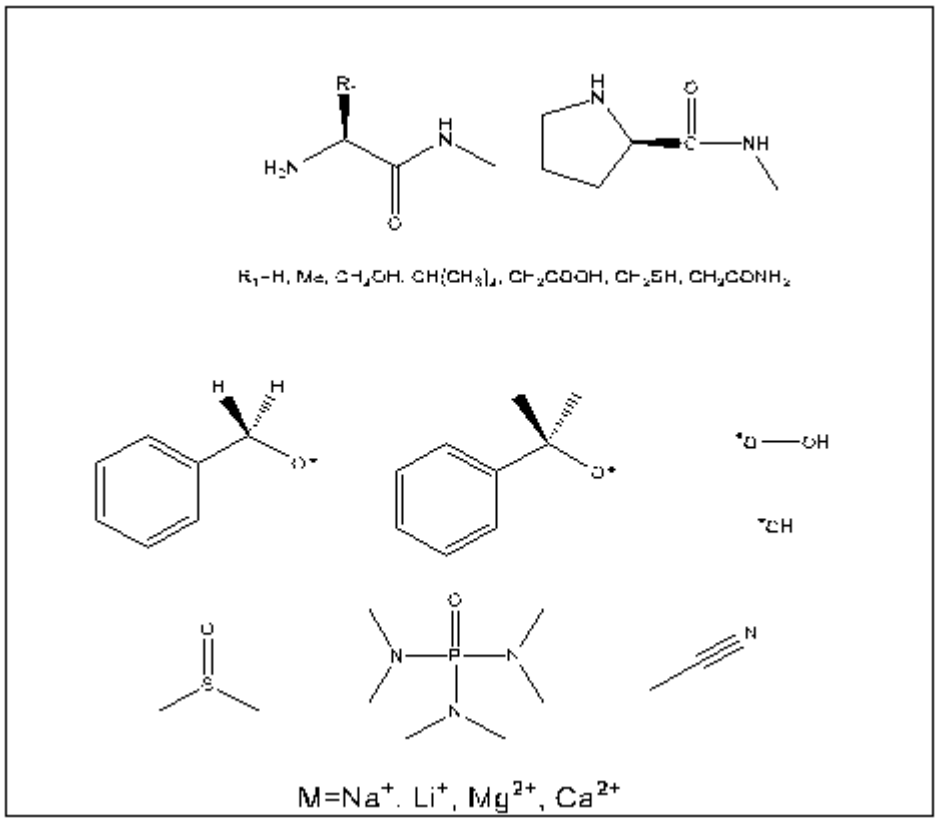

Scheme 6.2: Initial proposed benchmark set of molecules and cations. Note this set consistes of all combinations of substrates and metal cation, thus there are 60 complexes in the set.

6.1.3 Metal cation basis set convergence

6.1.4 High level results and evaluation of various density-functional theory methods

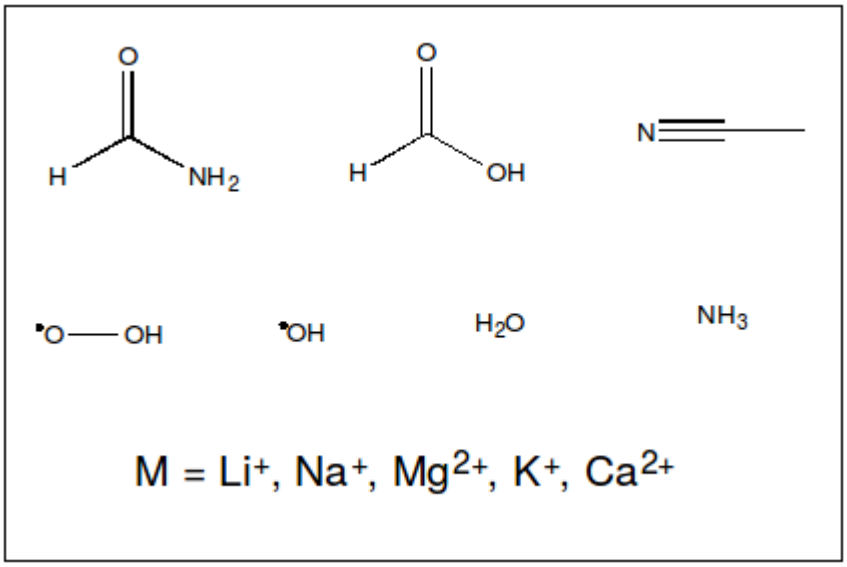

Scheme 6.3: Revised benchmark set of small substrates and cations. Note this set consistes of all combinations of substrates and metal cation, thus there are 35 complexes in the set.

Chapter 7

Conclusion

Here comes the conclusion.

Your conclusion can go on for several pages.

References

[1] Kochi, J., Ed. *Free Radicals, Vols. 1 and 2*; Wiley, New York, 1973.

[2] Parsons, A. F. *An Introduction to Free Radical Chemistry*; Wiley-Blackwell, 2000.

[3] Halliwell, B.; Gutteridge, J. M. *Free Radicals in Biology and Medicine*; Oxford University Press, USA, 2015.

[4] Barnham, K. J.; Masters, C. L.; Bush, A. I. Neurodegenerative diseases and oxidative stress. *Nat. Rev. Drug Discovery* **2004**, *3*, 205–214.

[5] Valko, M.; Leibfritz, D.; Moncol, J.; Cronin, M. T. D.; Mazur, M.; Telser, J. Free radicals and antioxidants in normal physiological functions and human disease. *International Journal of Biochemistry & Cell Biology* **2007**, *39*, 44–84.

[6] Hwang, O. Role of oxidative stress in Parkinson's disease. *Experimental Neurobiology* **2013**, *22*, 11–17.

[7] Halliwell, B. Oxidative stress and cancer: have we moved forward? *401*, 1–11.

[8] Sies, H. Strategies of antioxidant defense. *Eur. J. Biochem.* **1993**, *215*, 213–219.

[9] Dizdaroglu, M. Oxidative damage to DNA in mammalian chromatin. *Mutation Research/DNAging* **1992**, *275*, 331–342.

[10] Cooke, M. S.; Evans, M. D.; Dizdaroglu, M.; Lunec, J. Oxidative DNA damage: mechanisms, mutation, and disease. *The FASEB Journal* **2003**, *17*, 1195–1214.

[11] Cheng, K. C.; Cahill, D. S.; Kasai, H.; Nishimura, S.; Loeb, L. A. 8-Hydroxyguanine, an abundant form of oxidative DNA damage, causes G—-T and A—-C substitutions. *J. Biol. Chem.* **1992**, *267*, 166–172.

[12] Friedberg, E. C.; Walker, G. C.; Siede, W.; Wood, R. D. *DNA repair and mutagenesis*; American Society for Microbiology Press, 2005.

[13] Marnett, L. J. Oxyradicals and DNA damage. *Carcinogenesis* **2000**, *21*, 361–370.

[14] Sevanian, A.; Ursini, F. Lipid peroxidation in membranes and low-density lipoproteins: similarities and differences. *Free Radical Biol. Med.* **2000**, *29*, 306–311.

[15] Pratt, D. A.; Mills, J. H.; Porter, N. A. Theoretical calculations of carbon- oxygen bond dissociation enthalpies of peroxyl radicals formed in the autoxidation of lipids. *J. Am. Chem. Soc.* **2003**, *125*, 5801–5810.

[16] Spiteller, G. The important role of lipid peroxidation processes in aging and age dependent diseases. *Mol. Biotechnol.* **2007**, *37*, 5–12.

[17] Ayala, A.; Muñoz, M. F.; Argüelles, S. Lipid peroxidation: production, metabolism, and signaling mechanisms of malondialdehyde and 4-hydroxy-2-nonenal. *Oxidative Medicine and Cellular Longevity* **2014**, *2014*.

[18] Berlett, B. S.; Stadtman, E. R. Protein Oxidation in Aging, Disease, and Oxidative Stress. **1997**, *272*, 20313–20316.

[19] Stadtman, E. R. Role of oxidant species in aging. *Curr. Med. Chem.* **2004**, *11*, 1105–1112.

[20] Mulder, P.; Korth, H.-G.; Pratt, D. A.; DiLabio, G. A.; Valgimigli, L.; Pedulli, G. F.; Ingold, K. U. Critical Re-evaluation of the O-H Bond Dissociation Enthalpy in Phenol. *J. Phys. Chem. A* **2005**, *109*, 2647–2655.

[21] Halliwell, B. Oxidative stress and neurodegeneration: where are we now? *J. Neurochem.* **2006**, *97*, 1634–1658.

[22] Hammes-Schiffer, S. Proton-coupled electron transfer: classification scheme and guide to theoretical methods. *Energy & Environmental Science* **2012**, *5*, 7696–7703.

[23] Balcells, D.; Clot, E.; Eisenstein, O.; Nova, A.; Perrin, L. Deciphering Selectivity in Organic Reactions: A Multifaceted Problem. *Acc. Chem. Res.* **2016**, *49*, 1070–1078.

[24] Miller, D. C.; Tarantino, K. T.; Knowles, R. R. Proton-Coupled Electron Transfer in Organic Synthesis: Fundamentals, Applications, and Opportunities. *Top. Curr. Chem* **2016**, *374*, 145–203.

[25] Godula, K.; Sames, D. CH bond functionalization in complex organic synthesis. *Science* **2006**, *312*, 67–72.

[26] Barton, D.; Beaton, J.; Geller, L.; Pechet, M. A new photochemical reaction. *J. Am. Chem. Soc.* **1960**, *82*, 2640–2641.

[27] Groves, J. T.; McClusky, G. A. Aliphatic hydroxylation via oxygen rebound. Oxygen transfer catalyzed by iron. *J. Am. Chem. Soc.* **1976**, *98*, 859–861.

[28] Mader, E. A.; Davidson, E. R.; Mayer, J. M. Large Ground-State Entropy Changes for Hydrogen Atom Transfer Reactions of Iron Complexes. *J. Am. Chem. Soc.* **2007**, *129*, 5153–5166.

[29] Howard, J. A.; Ingold, K. U. THE INHIBITED AUTOXIDATION OF STYREN: PART IV. SOLVENT EFFECTS. *Can. J. Chem.* **1964**, *42*, 1044–1056.

[30] See Litwinienko, G.; Ingold, K. U. Solvent Effects on the Rates and Mech- anisms of Reaction of Phenols with Free Radicals. *Acc. Chem. Res.* **2007**, *40*, 222230, and references therein.

[31] Salamone, M.; Mangiacapra, L.; Bietti, M. Kinetic Solvent Effects on the Reactions of the Cumyloxyl Radical with Tertiary Amides. Control over the Hydrogen Atom Transfer Reactivity and Selectivity through Solvent Polarity and Hydrogen Bonding. *J. Org. Chem.* **2015a**, *80*, 1149–1154.

[32] Salamone, M.; Bietti, M. Reaction Pathways of Alkoxyl Radicals. The Role of Solvent Effects on C–C Bond Fragmentation and Hydrogen Atom Transfer Reactions. *Synlett* **2014**, *25*, 1803–1816.

[33] Bietti, M.; Martella, R.; Salamone, M. Understanding Kinetic Solvent Effects on Hydrogen Abstraction Reactions from Carbon by the Cumyloxyl Radical. *Org. Lett.* **2011**, *13*, 6110–6113.

[34] Bietti, M.; Salamone, M. Kinetic Solvent Effects on Hydrogen Abstraction Reactions from Carbon by the Cumyloxyl Radical. The Role of Hydrogen Bonding. *Org. Lett.* **2010**, *12*, 3654–3657.

[35] Johnson, E. R.; Dilabio, G. A. Radicals as hydrogen bond donors and acceptors. *Interdisciplinary Sciences: Computational Life Sciences* **2009**, *1*, 133–140.

[36] DiLabio, G. A.; Ingold, K. U. A Theoretical Study of the Iminoxyl/Oxime Self-Exchange Reaction. A Five-Center, Cyclic Proton-Coupled Electron Transfer. *127*, 6693–6699.

[37] DiLabio, G. A.; Johnson, E. R. Lone Pair-π and π-π Interactions Play an Important Role in Proton-Coupled Electron Transfer Reactions. *129*, 6199–6203.

[38] Uyeda, C.; Jacobsen, E. N. Transition-State Charge Stabilization through Multiple Non-covalent Interactions in the Guanidinium-Catalyzed Enantioselective Claisen Rearrangement. *J. Am. Chem. Soc.* **2011**, *133*, 5062–5075.

[39] Bakr, B. W.; Sherrill, C. D. Analysis of transition state stabilization by non-covalent interactions in the Houk–List model of organocatalyzed intermolecular Aldol additions using functional-group symmetry-adapted perturbation theory. *Phys. Chem. Chem. Phys.* **2016**, *18*, 10297–10308.

[40] Salamone, M.; Anastasi, G.; Bietti, M.; DiLabio, G. A. Diffusion Controlled Hydrogen Atom Abstraction from Tertiary Amines by the Benzyloxyl Radical. The Importance of C-H/N Hydrogen Bonding. *Org. Lett. 13*, 260–263.

[41] Salamone, M.; DiLabio, G. A.; Bietti, M. Hydrogen Atom Abstraction Reactions from Tertiary Amines by Benzyloxyl and Cumyloxyl Radicals: Influence of Structure on the Rate-Determining Formation of a Hydrogen-Bonded Prereaction Complex. *J. Org. Chem. 76*, 6264–6270.

[42] Salamone, M.; Milan, M.; DiLabio, G. A.; Bietti, M. Reactions of the Cumyloxyl and Benzyloxyl Radicals with Tertiary Amides. Hydrogen Abstraction Selectivity and the Role of Specific Substrate-Radical Hydrogen Bonding. *J. Org. Chem.* **2013**, *78*, 5909–5917.

[43] Tedder, J. M. Which factors determine the reactivity and regioselectivity of free radical substitution and addition reactions? *Angew. Chem. Int. Ed.* **1982**, *21*, 401–410.

[44] Wijtmans, M.; Pratt, D. A.; Valgimigli, L.; DiLabio, G. A.; Pedulli, G. F.; Porter, N. A. 6-Amino-3-Pyridinols: Towards Diffusion-Controlled Chain-Breaking Antioxidants. *Angew. Chem. Int. Ed.* **2003**, *42*, 4370–4373.

[45] Pratt, D. A.; DiLabio, G. A.; Mulder, P.; Ingold, K. U. Bond Strengths of Toluenes, Anilines, and Phenols: To Hammett or Not. *37*, 334–340.

[46] Mayer, J. M. Proton-coupled electron transfer: a reaction chemist's view. *Annu. Rev. Phys. Chem.* **2004**, *55*, 363–390.

[47] Anslyn, E. V.; Dougherty, D. A. *Modern physical organic chemistry*; University Science Books, 2006.

[48] Hammett, L. P. The effect of structure upon the reactions of organic compounds. Benzene derivatives. *J. Am. Chem. Soc.* **1937**, *59*, 96.

[49] Brown, H. C.; Okamoto, Y. Electrophilic Substituent Constants. *J. Am. Chem. Soc.* **1958**, *80*, 4979–4987.

[50] Bell, R. P. The Theory of Reactions Involving Proton Transfers. *Proceedings of the Royal Society A: Mathematical, Physical and Engineering Sciences* **1936**, *154*, 414–429.

[51] Evans, M. G.; Polanyi, M. Inertia and driving force of chemical reactions. *Trans. Faraday Soc.* **1938**, *34*, 11.

[52] Roberts, B. P. Polarity-reversal catalysis of hydrogen-atom abstraction reactions: concepts and applications in organic chemistry. *Chem. Soc. Rev.* **1999**, *28*, 25–35.

[53] Salamone, M.; Bietti, M. Tuning Reactivity and Selectivity in Hydrogen Atom Transfer from Aliphatic C–H Bonds to Alkoxyl Radicals: Role of Structural and Medium Effects. *Acc. Chem. Res.* **2015**, *48*, 2895–2903.

[54] Salamone, M.; DiLabio, G. A.; Bietti, M. Reactions of the Cumyloxyl and Benzyloxyl Radicals with Strong Hydrogen Bond Acceptors. Large Enhancements in Hydrogen Abstraction Reactivity Determined by Substrate/Radical Hydrogen Bonding. *J. Org. Chem. 77*, 10479–10487.

[55] Finn, M.; Friedline, R.; Suleman, N. K.; Wohl, C. J.; Tanko, J. M. Chemistry of thet-Butoxyl Radical: Evidence that Most Hydrogen

Abstractions from Carbon are Entropy-Controlled. *J. Am. Chem. Soc.* **2004**, *126*, 7578–7584.

[56] Pischel, U.; Nau, W. M. Switch-Over in Photochemical Reaction Mechanism from Hydrogen Abstraction to Exciplex-Induced Quenching: Interaction of Triplet-Excited versus Singlet-Excited Acetone versus Cumyloxyl Radicals with Amines. *J. Am. Chem. Soc.* **2001**, *123*, 9727–9737.

[57] Griller, D.; Howard, J. A.; Marriott, P. R.; Scaiano, J. C. Absolute rate constants for the reactions of tert-butoxyl, tert-butylperoxyl, and benzophenone triplet with amines: the importance of a stereoelectronic effect. *J. Am. Chem. Soc.* **1981**, *103*, 619–623.

[58] Malatesta, V.; Scaiano, J. C. Absolute rate constants for the reactions of tert-butoxyl with ethers: importance of the stereoelectronic effect. *J. Org. Chem.* **1982**, *47*, 1455–1459.

[59] Salamone, M.; Milan, M.; DiLabio, G. A.; Bietti, M. Absolute Rate Constants for Hydrogen Atom Transfer from Tertiary Amides to the Cumyloxyl Radical: Evaluating the Role of Stereoelectronic Effects. *J. Org. Chem.* **2014**, *79*, 7179–7184.

[60] Not to be confused with the net reaction of hydrogen atom transfer. The abbreviation HAT will be used interchangeably, although the distinction should be clear from context.

[61] Cukier, R. I.; Nocera, D. G. Proton-coupled electron transfer. *Annu. Rev. Phys. Chem.* **1998**, *49*, 337–369.

[62] Mayer, J. M.; Hrovat, D. A.; Thomas, J. L.; Borden, W. T. Proton-coupled electron transfer versus hydrogen atom transfer in benzyl/toluene, methoxyl/methanol, and phenoxyl/phenol self-exchange reactions. *J. Am. Chem. Soc.* **2002**, *124*, 11142–11147.

[63] Stubbe, J.; Nocera, D. G.; Yee, C. S.; Chang, M. C. Radical initiation in the class I ribonucleotide reductase: long-range proton-coupled electron transfer? *Chem. Rev.* **2003**, *103*, 2167–2202.

[64] Huynh, M. H. V.; Meyer, T. J. Proton-coupled electron transfer. *Chem. Rev.* **2007**, *107*, 5004–5064.

[65] Hammes-Schiffer, S.; Soudackov, A. V. Proton-coupled electron transfer in solution, proteins, and electrochemistry. *J. Phys. Chem. B* **2008**, *112*, 14108–14123.

[66] Mayer, J. M. Understanding hydrogen atom transfer: from bond strengths to Marcus theory. *Acc. Chem. Res.* **2010**, *44*, 36–46.

[67] Weinberg, D. R.; Gagliardi, C. J.; Hull, J. F.; Murphy, C. F.; Kent, C. A.; Westlake, B. C.; Paul, A.; Ess, D. H.; McCafferty, D. G.; Meyer, T. J. Proton-coupled electron transfer. *Chem. Rev.* **2012**, *112*, 4016–4093.

[68] Hammes-Schiffer, S. Proton-coupled electron transfer: Moving together and charging forward. *J. Am. Chem. Soc.* **2015**, *137*, 8860–8871.

[69] Muñoz-Rugeles, L.; Galano, A.; Alvarez-Idaboy, J. R. Non-Covalent π-π Stacking Interactions Turn Off Non-Adiabatic Effects in Proton-Coupled Electron Transfer Reactions. *Phys. Chem. Chem. Phys.* **2017**,

[70] Hatcher, E.; Soudackov, A. V.; Hammes-Schiffer, S. Proton-coupled electron transfer in soybean lipoxygenase: dynamical behavior and temperature dependence of kinetic isotope effects. *J. Am. Chem. Soc.* **2007**, *129*, 187–196.

[71] Karp, G. *Cell and Molecular Biology*; JOHN WILEY & SONS INC, 2013.

[72] Salamone, M.; Mangiacapra, L.; DiLabio, G. A.; Bietti, M. Effect of Metal Ions on the Reactions of the Cumyloxyl Radical with Hydrogen Atom Donors. Fine Control on Hydrogen Abstraction Reactivity Determined by Lewis Acid–Base Interactions. *J. Am. Chem. Soc.* **2013**, *135*, 415–423.

[73] Salamone, M.; Mangiacapra, L.; Carboni, G.; Bietti, M. Hydrogen atom transfer from tertiary alkanamides to the cumyloxyl radical. The role of substrate structure on alkali and alkaline earth metal ion induced C–H bond deactivation. *Tetrahedron* **2016**,

[74] Nova, A.; Balcells, D. Does the metal protect the ancillary ligands? C–H strengthening and deactivation in amines and phosphines upon metal-binding. *Chem. Commun.* **2014**, *50*, 614–616.

[75] Salamone, M.; Basili, F.; Bietti, M. Reactivity and Selectivity Patterns in Hydrogen Atom Transfer from Amino Acid C–H Bonds to the Cumyloxyl Radical: Polar Effects as a Rationale for the Preferential Reaction at Proline Residues. *J. Org. Chem.* **2015**, *80*, 3643–3650.

[76] Griffiths, D. J. *Introduction to quantum mechanics*; Cambridge University Press, 2016.

[77] Heisenberg, W. Mehrkörperproblem und Resonanz in der Quantenmechanik. *Zeitschrift für Physik* **1926**, *38*, 411–426.

[78] Dirac, P. A. M. On the Theory of Quantum Mechanics. *Proceedings of the Royal Society A: Mathematical, Physical and Engineering Sciences* **1926**, *112*, 661–677.

[79] Slater, J. C. The Theory of Complex Spectra. *Phys. Rev.* **1929**, *34*, 1293–1322.

[80] Roothaan, C. C. J. New Developments in Molecular Orbital Theory. *Rev. Mod. Phys.* **1951**, *23*, 69–89.

[81] Gill, P. M. *Advances in Quantum Chemistry*; Elsevier BV, 1994; pp 141–205.

[82] Szabo, A.; Ostlund, N. S. Modern Quantum Chemistry: Intro to Advanced Electronic Structure Theory. **1996**,

[83] Jensen, F. Atomic orbital basis sets. *WIREs Comput Mol Sci* **2012**, *3*, 273–295.

[84] Hehre, W. J.; Stewart, R. F.; Pople, J. A. Self-Consistent Molecular-Orbital Methods. I. Use of Gaussian Expansions of Slater-Type Atomic Orbitals. *The Journal of Chemical Physics* **1969**, *51*, 2657–2664.

[85] Dunning, T. H. Gaussian basis sets for use in correlated molecular calculations. I. The atoms boron through neon and hydrogen. *J. Chem. Phys.* **1989**, *90*, 1007–1023.

[86] Jensen, F. Polarization consistent basis sets: Principles. *115*, 9113.

[87] Schäfer, A.; Horn, H.; Ahlrichs, R. Fully optimized contracted Gaussian basis sets for atoms Li to Kr. *J. Chem. Phys.* **1992**, *97*, 2571–2577.

[88] TURBOMOLE V6.3 2011, a development of University of Karlsruhe and Forschungszentrum Karlsruhe GmbH, 1989-2007, TURBOMOLE GmbH, since 2007; available from `http://www.turbomole.com`.

[89] Cramer, C. J. *Essentials of Computational Chemistry*; Wiley John + Sons, 2004.

[90] Crawford, T. D.; Schaefer, H. F. *Reviews in Computational Chemistry*; Wiley-Blackwell, 2000; pp 33–136.

[91] Levine, I. N. *Quantum Chemistry*; Prentice Hall, 2013.

[92] Truhlar, D. G. Basis-set extrapolation. *Chem. Phys. Lett.* **1998**, *294*, 45–48.

[93] Feller, D. Application of systematic sequences of wave functions to the water dimer. *J. Chem. Phys.* **1992**, *96*, 6104–6114.

[94] Feller, D. The use of systematic sequences of wave functions for estimating the complete basis set, full configuration interaction limit in water. *J. Chem. Phys.* **1993**, *98*, 7059–7071.

[95] Helgaker, T.; Klopper, W.; Koch, H.; Noga, J. Basis-set convergence of correlated calculations on water. *J. Chem. Phys.* **1997**, *106*, 9639–9646.

[96] Halkier, A.; Helgaker, T.; Jørgensen, P.; Klopper, W.; Koch, H.; Olsen, J.; Wilson, A. K. Basis-set convergence in correlated calculations on Ne, N2, and H2O. *Chem. Phys. Lett.* **1998**, *286*, 243–252.

[97] Kupka, T.; Lim, C. Polarization-Consistent versus Correlation-Consistent Basis Sets in Predicting Molecular and Spectroscopic Properties. *J. Phys. Chem. A* **2007**, *111*, 1927–1932.

[98] Shiozaki, T.; Kamiya, M.; Hirata, S.; Valeev, E. F. Explicitly correlated coupled-cluster singles and doubles method based on complete diagrammatic equations. *J. Chem. Phys.* **2008**, *129*, 071101.

[99] Köhn, A.; Richings, G. W.; Tew, D. P. Implementation of the full explicitly correlated coupled-cluster singles and doubles model CCSD-F12 with optimally reduced auxiliary basis dependence. *J. Chem. Phys.* **2008**, *129*, 201103.

[100] Ten-no, S.; Noga, J. Explicitly correlated electronic structure theory from R12/F12 anstze. *WIREs Comput Mol Sci* **2012**, *2*, 114–125.

[101] Feller, D. Benchmarks of improved complete basis set extrapolation schemes designed for standard CCSD(T) atomization energies. *J. Chem. Phys.* **2013**, *138*, 074103.

[102] Karton, A. A computational chemist's guide to accurate thermochemistry for organic molecules. *WIREs Comput Mol Sci* **2016**, *6*, 292–310.

[103] Curtiss, L. A.; Redfern, P. C.; Raghavachari, K. Gaussian-4 theory. *J. Chem. Phys.* **2007**, *126*, 084108.

[104] Curtiss, L. A.; Redfern, P. C.; Raghavachari, K. Gaussian-4 theory using reduced order perturbation theory. *J. Chem. Phys.* **2007**, *127*, 124105.

[105] Montgomery, J. A.; Frisch, M. J.; Ochterski, J. W.; Petersson, G. A. A complete basis set model chemistry. VI. Use of density functional geometries and frequencies. *J. Chem. Phys.* **1999**, *110*, 2822–2827.

[106] Montgomery, J. A.; Frisch, M. J.; Ochterski, J. W.; Petersson, G. A. A complete basis set model chemistry. VII. Use of the minimum population localization method. *J. Chem. Phys.* **2000**, *112*, 6532–6542.

[107] Ochterski, J. W.; Petersson, G. A.; Montgomery, J. A. A complete basis set model chemistry. V. Extensions to six or more heavy atoms. *J. Chem. Phys.* **1996**, *104*, 2598–2619.

[108] Barnes, E. C.; Petersson, G. A.; Montgomery, J. A.; Frisch, M. J.; Martin, J. M. L. Unrestricted Coupled Cluster and Brueckner Doubles Variations of W1 Theory. *J. Chem. Theory Comput.* **2009**, *5*, 2687–2693.

[109] Hohenberg, P.; Kohn, W. Inhomogeneous Electron Gas. *Phys. Rev.* **1964**, *136*, B864–B871.

[110] Koch, W.; Holthausen, M. C. *A Chemist's Guide to Density Functional Theory: An Introduction*; Wiley-VCH, 2000.

[111] Kohn, W.; Sham, L. J. Self-Consistent Equations Including Exchange and Correlation Effects. *Phys. Rev.* **1965**, *140*, A1133–A1138.

[112] Becke, A. D. Density-functional thermochemistry. III. The role of exact exchange. *J. Chem. Phys.* **1993**, *98*, 5648–5652.

[113] Lee, C.; Yang, W.; Parr, R. G. Development of the Colle-Salvetti correlation-energy formula into a functional of the electron density. *Phys. Rev. B* **1988**, *37*, 785–789.

[114] Zhao, Y.; Schultz, N. E.; Truhlar, D. G. Design of Density Functionals by Combining the Method of Constraint Satisfaction with Parametrization for Thermochemistry, Thermochemical Kinetics, and Noncovalent Interactions. *J. Chem. Theory Comput.* **2006**, *2*, 364–382.

[115] Zhao, Y.; Truhlar, D. G. The M06 suite of density functionals for main group thermochemistry, thermochemical kinetics, noncovalent interactions, excited states, and transition elements: two new functionals and systematic testing of four M06-class functionals and 12 other functionals. *Theor. Chem. Acc.* **2006**, *120*, 215–241.

[116] Yanai, T.; Tew, D. P.; Handy, N. C. A new hybrid exchange–correlation functional using the Coulomb-attenuating method (CAM-B3LYP). *Chem. Phys. Lett.* **2004**, *393*, 51–57.

[117] Cohen, A. J.; Mori-Sánchez, P.; Yang, W. Challenges for Density Functional Theory. *Chem. Rev.* **2012**, *112*, 289–320.

[118] DiLabio, G. A.; Otero-de-la-Roza, A. *Reviews in Computational Chemistry*; Wiley-Blackwell, 2016; pp 1–97.

[119] Grimme, S.; Antony, J.; Ehrlich, S.; Krieg, H. A consistent and accurate ab initio parametrization of density functional dispersion correction (DFT-D) for the 94 elements H-Pu. *The Journal of Chemical Physics* **2010**, *132*, 154104.

[120] Johnson, E. R.; Becke, A. D. A post-Hartree-Fock model of intermolecular interactions: Inclusion of higher-order corrections. *J. Chem. Phys.* **2006**, *124*, 174104.

[121] Mori-Sánchez, P.; Cohen, A. J.; Yang, W. Localization and Delocalization Errors in Density Functional Theory and Implications for Band-Gap Prediction. *Phys. Rev. Lett.* **2008**, *100*.

[122] Otero-de-la-Roza, A.; Johnson, E. R.; DiLabio, G. A. Halogen Bonding from Dispersion-Corrected Density-Functional Theory: The Role of Delocalization Error. *J. Chem. Theory Comput.* **2014**, *10*, 5436–5447.

[123] Heidrich, D.; Kliesch, W.; Quapp, W. *Properties of Chemically Interesting Potential Energy Surfaces*; Springer Berlin Heidelberg, 1991.

[124] Wilson, E. B.; Decius, J. C.; Cross, P. C. *Molecular Vibrations: The Theory of Infrared and Raman Vibrational Spectra (Dover Books on Chemistry)*; Dover Publications, 1980.

[125] McQuarrie, D. A.; Simon, J. D. *Molecular Thermodynamics*; University Science Books, 1999.

[126] McQuarrie, D. A. *Statistical Mechanics*; UNIV SCIENCE BOOKS, 2000.

[127] Note that Q is actually a function of the number of moles, volume of a system, and temperature. This description, denoted as $Q(N, V, T)$ has been omitted for simplicity.

[128] Mennucci, B., Cammi, R., Eds. *Continuum Solvation Models in Chemical Physics: From Theory to Applications*; John Wiley & Sons Inc., 2007.

[129] Marenich, A. V.; Cramer, C. J.; Truhlar, D. G. Universal Solvation Model Based on Solute Electron Density and on a Continuum Model of the Solvent Defined by the Bulk Dielectric Constant and Atomic Surface Tensions. *J. Phys. Chem. B* **2009**, *113*, 6378–6396.

[130] Ho, J.; Klamt, A.; Coote, M. L. Comment on the Correct Use of Continuum Solvent Models. *J. Phys. Chem. A* **2010**, *114*, 13442–13444.

[131] McQuarrie, D. A.; Simon, J. D. *Physical Chemistry: A Molecular Approach*; University Science Books, 1997.

[132] Steinfeld, J. I.; Francisco, J. S.; Hase, W. L. *Chemical Kinetics and Dynamics*, 2nd ed.; Prentice Hall, 1998.

[133] Truhlar, D. G.; Garrett, B. C. Variational Transition State Theory. *Annu. Rev. Phys. Chem.* **1984**, *35*, 159–189.

[134] Bell, R. P. *The Tunnel Effect in Chemistry*; Springer Nature, 1980.

[135] Johnston, H. S.; Heicklen, J. Tunnelling Corrections For Unsymmetrical Eckart Potential Energy Barriers. *J. Phys. Chem.* **1962**, *66*, 532–533.

[136] Frisch, M. J. et al. Gaussian 09, Revision D. 01. 2009.

[137] Dennington, R.; Keith, T. A.; Millam, J. M. GaussView Version 5. 2009; Semichem Inc. Shawnee Mission KS.

[138] Andrienko, G. A. Chemcraft. 2015; http://www.chemcraftprog.com.

[139] Becke, A. D. Density-functional exchange-energy approximation with correct asymptotic behavior. *Phys. Rev. A* **1988**, *38*, 3098–3100.

[140] Andzelm, J.; Klobukowski, M.; Radzio-andzelm, E.; Sakai, Y.; Tatewaki, H. In *Gaussian Basis Sets For Molecular Calculation*; Huzinaga, S., Ed.; Elsevier, 1984; Valence Scale Factors From John Deisz Of North Dakota State University.

[141] The Escher program[154] was used to generate a Z-matrix with specific dihedral angles. This geometry was then systematically scanned using simple shell scripts.

[142] Vydrov, O. A.; Scuseria, G. E. Assessment of a long-range corrected hybrid functional. *J. Chem. Phys.* **2006**, *125*, 234109.

[143] Vydrov, O. A.; Heyd, J.; Krukau, A. V.; Scuseria, G. E. Importance of short-range versus long-range Hartree-Fock exchange for the performance of hybrid density functionals. *J. Chem. Phys.* **2006**, *125*, 074106.

[144] Johnson, E. R.; Otero-de-la-Roza, A.; Dale, S. G.; DiLabio, G. A. Efficient basis sets for non-covalent interactions in XDM-corrected density-functional theory. *J. Chem. Phys.* **2013**, *139*, 214109.

[145] Luo, Y.-R. *Handbook of Bond Dissociation Energies in Organic Compounds*; CRC Press, 2002.

[146] Bordwell, F.; Cheng, J. P.; Harrelson, J. A. Homolytic bond dissociation energies in solution from equilibrium acidity and electrochemical data. *J. Am. Chem. Soc.* **1988**, *110*, 1229–1231.

[147] Johnson, E. R.; Salamone, M.; Bietti, M.; DiLabio, G. A. Modeling Noncovalent Radical–Molecule Interactions Using Conventional Density-Functional Theory: Beware Erroneous Charge Transfer. *J Phys Chem A* **2013**, *117*, 947–952.

[148] Hättig, C.; Tew, D. P.; Köhn, A. Accurate and efficient approximations to explicitly correlated coupled-cluster singles and doubles, CCSD-F12. *J. Chem. Phys.* **2010**, *132*, 231102.

[149] Galano, A.; Alvarez-Idaboy, J. R. A computational methodology for accurate predictions of rate constants in solution: Application to the

assessment of primary antioxidant activity. *J. Comput. Chem.* **2013**, *34*, 2430–2445.

[150] Dutoi, A. D.; Head-Gordon, M. Self-interaction error of local density functionals for alkali–halide dissociation. *Chem. Phys. Lett.* **2006**, *422*, 230–233.

[151] Johnson, E. R.; Mackie, I. D.; DiLabio, G. A. Dispersion interactions in density-functional theory. *J. Phys. Org. Chem.* **2009**, *22*, 1127–1135.

[152] Suárez, D.; Rayón, V. M.; Díaz, N.; Valdés, H. Ab initio benchmark calculations on Ca (II) complexes and assessment of density functional theory methodologies. *115*, 11331–11343.

[153] Harding, M. M. The geometry of metal–ligand interactions relevant to proteins. *Acta Crystallogr., Sect. D: Biol. Crystallogr.* **1999**, *55*, 1432–1443.

[154] Otero-de-la-Roza, A. Escher. Accessed Apr. 3, 2017: https://github.com/aoterodelaroza/escher.

Appendix